

**UNCLASSIFIED**

**AD 4 5 2 9 5 8**

**DEFENSE DOCUMENTATION CENTER**

**FOR**

**SCIENTIFIC AND TECHNICAL INFORMATION**

**CAMERON STATION ALEXANDRIA, VIRGINIA**



**UNCLASSIFIED**

NOTICE: When government or other drawings, specifications or other data are used for any purpose other than in connection with a definitely related government procurement operation, the U. S. Government thereby incurs no responsibility, nor any obligation whatsoever; and the fact that the Government may have formulated, furnished, or in any way supplied the said drawings, specifications, or other data is not to be regarded by implication or otherwise as in any manner licensing the holder or any other person or corporation, or conveying any rights or permission to manufacture, use or sell any patented invention that may in any way be related thereto.

UNCLASSIFIED BY DDC  
AS AD No.

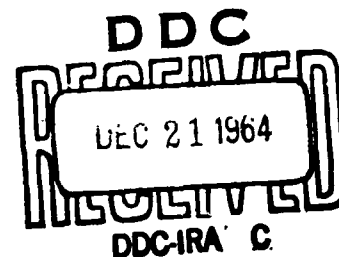
452958

452958

USNRDL-TR-790  
6 October 1964

EXPERIMENTAL DETERMINATION OF  
THE GAMMA-RAY ANGULAR DOSE ALBEDOS OF  
CONCRETE, ALUMINUM AND STEEL

by  
T. H. Jones  
N. E. Scofield  
L. G. Haggmark  
W. J. Gurney



NOT TO BE RELEASED  
TO OTS

U.S. NAVAL RADIOLOGICAL  
DEFENSE LABORATORY

SAN FRANCISCO • CALIFORNIA • 94135

NUCLEAR RADIATION PHYSICS BRANCH  
J. M. Ferguson, Head

NUCLEONICS DIVISION  
W. E. Kreger, Head

---

ADMINISTRATIVE INFORMATION

This report covers a portion of the work authorized by the Bureau of Ships, Subproject SF 011 05 11, Task 0501, and by the Defense Atomic Support Agency, NWER A-2, Subtask 11.038.

ACKNOWLEDGMENTS


The authors gratefully acknowledge their indebtedness to R. A. Taylor for his development of necessary electronic components of the dosimetry system used in this experiment. The authors further wish to acknowledge the assistance received from R. L. Green, M. B. Hastings, and W. D. Myers in the preparation and execution of the experiment.

DDC AVAILABILITY NOTICE

Qualified requesters may obtain copies of this report from DDC.

---

*Edward R. Tompkins*  
Edward R. Tompkins  
Associate Scientific Director

  
D.C. Campbell, CAPT USN  
Commanding Officer and Director

## ABSTRACT

The angular distribution of dose albedo was measured for "semi-infinite" concrete, aluminum and steel slabs irradiated by plane-parallel beams of  $\text{Co}^{60}$  and  $\text{Cs}^{137}$  gamma photons. The photons were incident on the slabs at angles, measured from a normal to the slab, of  $\arccos 1.00$ ,  $0.75$  and  $0.50$ . For the necessary sensitivity, the reflected dose rate was measured by a digital dosimetry system using a plastic scintillator as the detector.

An empirical formula for angular dose albedo was derived from the experimental data. Comparisons are made with the Monte Carlo calculations of D. J. Raso and the experimental results of C. E. Clifford (DRCL).

## SUMMARY

In many shielding problems it is important to know the amount of gamma radiation "reflected" (backscattered) from a surface relative to that which is incident upon the surface. This quantity, when measured in terms of dose, is referred to as dose albedo. In this experiment dose albedos have been measured for thick slabs of concrete, aluminum and steel at various angles relative to the perpendicular to the slab's surface. Two gamma-ray sources,  $\text{Co}^{60}$  and  $\text{Cs}^{137}$ , were each used to irradiate the slabs at three angles of incidence.

In order to facilitate the solution of those shielding problems which involve backscattered gamma radiation, a simple mathematical expression has been derived from the experimental data. The experimental data have also been compared with theoretical calculations that use the Monte Carlo technique. In general, the experimental results are higher than the theoretical calculations and, in some cases, exceed the theoretical values by more than 50 percent.

## CONTENTS

	<u>Page</u>
ADMINISTRATIVE INFORMATION . . . . .	inside front cover
ACKNOWLEDGMENTS . . . . .	inside front cover
ABSTRACT . . . . .	1
SUMMARY . . . . .	11
LIST OF FIGURES . . . . .	v-vi
LIST OF TABLES . . . . .	vii
GLOSSARY . . . . .	viii
I. INTRODUCTION . . . . .	1
II. DOSIMETRY SYSTEM . . . . .	2
III. DATA PRESENTATION . . . . .	2
A. Calculation of $\alpha_d(\vec{n})$ . . . . .	2
B. Tabulated Data . . . . .	6
IV. DATA ANALYSIS . . . . .	17
A. Concrete . . . . .	17
B. Aluminum and Steel . . . . .	27
V. ERROR ESTIMATION AND DISCUSSION OF RESULTS . . . . .	29
A. Systematic Error . . . . .	29
B. Relative Error . . . . .	29
C. Discussion and Comparisons . . . . .	29
APPENDIX I. DISCUSSION OF ALBEDO . . . . .	34
A. General . . . . .	34
B. Notation . . . . .	34
C. Definitions . . . . .	34

## CONTENTS (cont'd)

	<u>Page</u>
D. Integral Albedo . . . . .	35
E. Differential Albedo . . . . .	37
 APPENDIX II. EXPERIMENTAL APPARATUS AND METHODS . . . . .	 39
A. Experimental Design . . . . .	39
B. Dosimetry System . . . . .	42
1. Detector . . . . .	42
2. Converter . . . . .	44
3. Register . . . . .	44
4. Reductor . . . . .	46
C. Preoperational Calibration . . . . .	46
1. ADC Calibration . . . . .	46
2. Linearity and Threshold . . . . .	47
D. Dosimetry System Calibration . . . . .	47
E. Data Acquisition and Recording . . . . .	52
 REFERENCES . . . . .	 53



# LIST OF FIGURES

<u>Figure</u>		<u>Page</u>
1	Coordinate System . . . . .	4
2	Graph of $A_d(\vec{n})$ versus $\theta_s$ ; Cs <sup>137</sup> , $\cos\theta_o = 0.75$ , concrete .	19
3	Graph of $A_d(\vec{n})$ versus $\theta_s$ ; Cs <sup>137</sup> , $\cos\theta_o = 0.50$ , concrete .	20
4	Graph of $A_d(\vec{n})$ versus $\theta_s$ ; Co <sup>60</sup> , $\cos\theta_o = 0.75$ , concrete .	21
5	Graph of $A_d(\vec{n})$ versus $\theta_s$ ; Co <sup>60</sup> , $\cos\theta_o = 0.50$ , concrete .	22
6	Semi-log graph of $[A_d(\vec{n})-b]$ versus $\theta_s$ ; Cs <sup>137</sup> , $\cos\theta_o =$ 0.75, concrete . . . . .	23
7	Semi-log graph of $[A_d(\vec{n})-b]$ versus $\theta_s$ ; Cs <sup>137</sup> , $\cos\theta_o =$ 0.50, concrete . . . . .	24
8	Semi-log graph of $[A_d(\vec{n})-b]$ versus $\theta_s$ ; Co <sup>60</sup> , $\cos\theta_o =$ 0.75, concrete . . . . .	25
9	Semi-log graph of $[A_d(\vec{n})-b]$ versus $\theta_s$ ; Co <sup>60</sup> , $\cos\theta_o =$ 0.50, concrete . . . . .	26
10	Graph of $[A_d(\vec{n})-b]$ versus $\theta_s$ ; all experimental data . . .	28
11	Comparison of Clifford with NRDL; $A_d(\vec{n})$ versus $\theta_s$ . . . .	31
12	Comparison of Chilton-Huddleston with NRDL; $A_d(\vec{n})$ versus $\theta_s$ . . . . .	32
13	Histograms of the Comparison Ratio Distributions . . . . .	33
14	Space Diagram . . . . .	36

# LIST OF FIGURES (cont'd)

<u>Figure</u>		<u>Page</u>
15a	Experimental Configuration . . . . .	40
15b	Slab-Detector Geometry . . . . .	41
15c	Irradiated and "Viewed" Areas of the Slab . . . . .	41
16	Dosimetry System Diagram . . . . .	43
17	Pulse-Height Distribution . . . . .	45
18	Linearity Calibration Curve . . . . .	48
19	Dosimetry System Calibration Geometry . . . . .	50
20	Energy Dependence of Dose Conversion Factor . . . . .	51

# LIST OF TABLES

<u>Table</u>		<u>Page</u>
1	Dose Albedo, $\alpha_d(\vec{n})$ ; Cs <sup>137</sup> , concrete . . . . .	7
2	Dose Albedo, $\alpha_d(\vec{n})$ ; Co <sup>60</sup> , concrete . . . . .	8
3	Calculated Dose Albedo, $\alpha_d$ ; Cs <sup>137</sup> , concrete . . . . .	9
4	Calculated Dose Albedo, $\alpha_d$ ; Co <sup>60</sup> , concrete . . . . .	10
5	Dose-Rate Ratio, $A_d(\vec{n})$ ; Cs <sup>137</sup> , concrete . . . . .	11
6	Dose-Rate Ratio, $A_d(\vec{n})$ ; Co <sup>60</sup> , concrete . . . . .	12
7	Dose Albedo, $\alpha_d(\vec{n})$ ; Cs <sup>137</sup> , aluminum . . . . .	13
8	Dose Albedo, $\alpha_d(\vec{n})$ ; Co <sup>60</sup> , aluminum . . . . .	14
9	Dose Albedo, $\alpha_d(\vec{n})$ ; Cs <sup>137</sup> , steel . . . . .	15
10	Dose Albedo, $\alpha_d(\vec{n})$ ; Co <sup>60</sup> , steel . . . . .	16
11	Empirical-Fit Parameters for Concrete Experimental A <sub>d</sub> ( $\vec{n}$ ) Values . . . . .	18

# GLOSSARY

$\alpha$	albedo (current-reflection coefficient)
$\alpha_d(\vec{n})$	angular dose albedo (Raso's $\alpha_d$ )
$\alpha_n$	number albedo
A	flux reflection coefficient
$A_d(\vec{n})$	angular dose reflection coefficient (Raso's dose-rate ratio, $A_d$ )
$a_e$	projection of the "viewed" slab area normal to detector axis
dD	detected dose rate (calculated by the reductor formula)
$\phi$	azimuth angle of detector
$\phi'$	azimuth angle of source
$h\nu$	scattered photon energy
$h\nu'$ or $h\nu_0$	primary or source photon energy
$h\nu_i$	<u>i</u> th calibration source photon energy
I	flux density
$I_d(\vec{n})$	angular dose rate
$I_d(\theta, \phi, h\nu)$	angular energy dose rate
$I_n(\theta, \phi, h\nu)$ or $I_n(\vec{n}, h\nu)$	angular energy flux density
$I_n(\vec{r}, \vec{n}, h\nu)$	angular energy flux density at the point $\vec{r}$
J	current density
$J_d(o)$	incident "dose-current"
$J_d(\vec{n})$	angular "dose-current"

## I. INTRODUCTION

This investigation is one of a series arising from the basic experimental shielding program at NRD. Previous studies have been concerned with transmitted gamma photon spectral and angular distribution,<sup>1</sup> with transmitted and reflected dose,<sup>2</sup> and with the angular distribution of transmitted dose.<sup>3</sup>

This report presents experimental measurements of the angular distribution of dose reflection coefficients (albedos) for "semi-infinite" concrete, aluminum and steel slabs irradiated by plane-parallel, monoenergetic gamma photons. The sources,  $\text{Co}^{60}$  and  $\text{Cs}^{137}$ , were each collimated to irradiate nearly all of the surface of a slab. A plastic scintillator was collimated to point at the center of a slab face and to "view" an area of a slab surface, which was small with respect to the irradiated surface area.

Since one of the objectives of this investigation was to provide an experimental verification of Raso's Monte Carlo calculations,<sup>4</sup> the polar angles,  $\theta$ , and azimuth angles,  $\phi$ , for detector positioning and incidence angles,  $\theta_0$ , for source positioning were chosen to correspond to those used by Raso.

An exact source energy correspondence was not feasible for Raso's choice of input energies. However, Chilton and Huddleston,<sup>5</sup> using a semi-empirical formula and Raso's data, have calculated dose albedos for  $\text{Co}^{60}$  and  $\text{Cs}^{137}$  source energies.\* These albedo values for concrete have been tabulated in this report for comparison.

The format of this report was adopted as an attempt to lead the reader to the results as quickly as possible. Details concerning the means by which these results were derived are relegated to the appendices. Appendix I contains the notation and definitions used in this report as well as a discussion of the concept of gamma-ray albedo. In Appendix II is found a discussion of the conditions imposed upon the

---

\* Private communication.

design of the experimental apparatus by the albedo quantity to be determined, and the methods by which they were satisfied.

## II. DOSIMETRY SYSTEM

The inputs to the dosimetry system are the reflected gamma-ray photons from the slab face. The system is composed of four sections: detector, converter, register, and reductor. The function of the detector section is to convert the energy deposited in the plastic scintillator by each interacting photon into an electrical pulse whose voltage amplitude is proportional to that energy. The function of the converter section is to amplify and convert these voltage pulses into digital pulses. In the conversion process a pulse train is generated, the number of pulses in the train being a digital representation of the deposited energy. Each conversion also gives rise to a pulse which is called an events pulse. In the register section the digital and events pulses are accumulated in the digital and events registers, respectively. In the reductor section these accumulated quantities are combined to determine detected dose rate, which is designated  $\dot{D}$  to conform with Rao's notation.

## III. DATA PRESENTATION

### A. Calculation of $\alpha_d(\vec{n})$

The quantity to be determined from the experimentally measured quantities is the differential angular dose albedo,  $\alpha_d(\vec{n})$ .  $\alpha_d(\vec{n})$  is defined\* as the ratio of  $J_d(\vec{n})$ , the differential angular "dose-current" scattered ("reflected") out of the slab, to  $(J_d)_0$ , the "dose-current" incident on the slab. In equation form:

---

\* See Discussion of Albedo, Appendix I.

$$\alpha_d(\vec{\Omega}) = \frac{J_d(\vec{\Omega}) \text{ keV/g.s.sr}}{(J_d)_o \text{ keV/g.s}}$$

The quantities measured were dD, the detected dose rate, and  $(I_d)_o$ , the dose flux incident on the slab. It is now necessary to establish the relationships between the measured and desired quantities.  $(J_d)_o$  is readily obtained from  $(I_d)_o$  by the relationship between current and flux. Therefore

$$(J_d)_o = (I_d)_o \cos \theta_o$$

where  $\theta_o$  is the angle between the source to slab center line and the slab normal as shown in Fig. 1.

In order to relate dD to  $J_d(\vec{\Omega})$  the following is noted: the radiation received by the detector is limited to that which is within a small but finite solid angle,  $\Omega_e$  (effective detector solid angle), defined by the detector collimator; further,  $I_d(\vec{\Omega})^*$  is the angular dose rate scattered from the slab and  $I_d(\vec{\Omega})d\Omega$  is the dose rate from the center of the slab in direction  $\vec{\Omega}$ , within the solid angle  $d\Omega$ . Therefore, the following relationship exists between dD and  $I_d(\vec{\Omega})$ .

$$dD = \int_0^{\Omega_e} I_d(\vec{\Omega}) d\Omega.$$

Now, assuming that  $I_d(\vec{\Omega})$  is constant in the integration interval,

$$dD = I_d(\vec{\Omega}) \Omega_e.$$

---

\* See Discussion of Albedo, Appendix I.

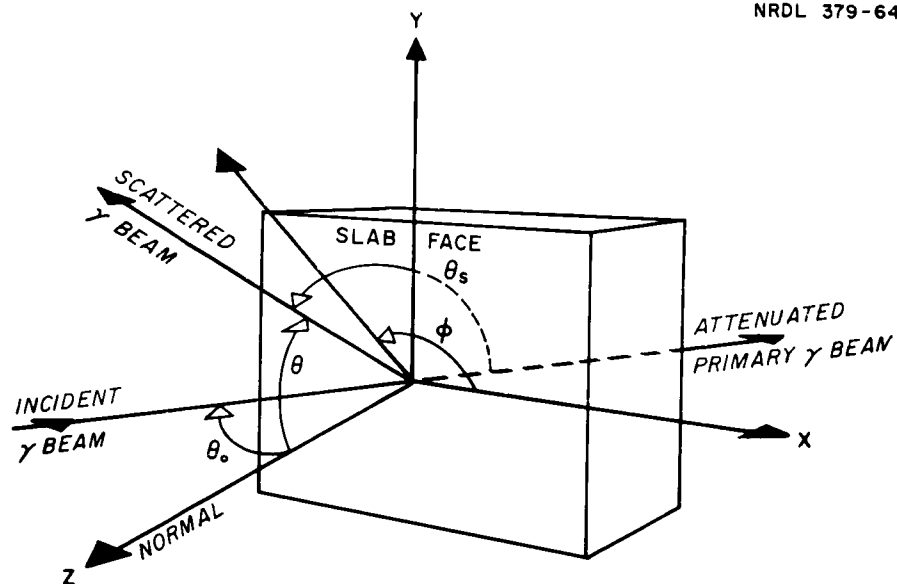


Fig. 1 Coordinate System.



Finally, using the relationship between flux and current quantities,

$$dD = \frac{J_d(\vec{n})}{\cos\theta} \Omega_\epsilon,$$

where  $\theta$  is the angle between the detector to slab center line and the slab normal as shown in Fig. 1.

Therefore, the desired relationship is

$$\alpha_d(\vec{n}) = \frac{dD \cos\theta}{\Omega_\epsilon (I_d)_o \cos\theta_o}.$$

A more "physical" quantity used in the analysis of the experimental data is  $A_d(\vec{n})$ . As stated by Raso,<sup>4</sup> "...  $A_d^*$  is the dose rate ratio [angular dose reflection coefficient] which would be physically observed by an infinitesimal directional detector embedded in the surface."  $A_d(\vec{n})$  is defined as follows:

$$A_d(\vec{n}) = \frac{\cos\theta_o}{\cos\theta} \alpha_d(\vec{n}).$$

Therefore

$$A_d(\vec{n}) = \frac{dD}{\Omega_\epsilon (I_d)_o}.$$

---

\* Raso uses  $A_d$  and  $\alpha_d$  where this report uses  $A_d(\vec{n})$  and  $\alpha_d(\vec{n})$ . Our notation is intended to alert the reader to the fact that the values are per steradian. Wherever values derived from Raso are quoted, his notation will be used.

## B. Tabulated Data

Tables 1 through 4 and 7 through 10 contain values of dose albedo and Tables 5 and 6 contain values of dose-rate ratio. The values are displayed as entries in arrays in which the column headings are the detector  $\theta$  values and the row headings are the detector  $\phi$  values. Each table contains three arrays, one for each source incidence angle,  $\theta_0$ . The arrays for  $\theta_0 = 0$  (normal incidence) have only one  $\phi$  row since in this case azimuthal symmetry prevails. The experimental values have been multiplied by  $10^4$  and the calculated values by  $10^5$  for presentation in the tables.

Tables 1 and 2 contain  $\alpha_d(\vec{n})$  values for 12 in. of concrete obtained from the experimental data. Tables 3 and 4 contain  $\alpha_d$  values predicted by Chilton-Huddleston formula based upon Raso's Monte Carlo calculation for a semi-infinite concrete medium. The Chilton-Huddleston formula is

$$\alpha_d = \frac{CK(\theta_s) 10^{26} + C'}{1 + \cos\theta_0 \sec\theta}$$

where  $K(\theta_s)$  is the Klein-Nishina differential energy scattering cross section for the scattering angle  $\theta_s$ .  $C$  and  $C'$  are fitting parameters.

In Tables 1, 3, 5, 7, 9 the monoenergetic source photon energy is 662 keV ( $\text{Cs}^{137}$ ). In Tables 2, 6, 8 and 10 the source was  $\text{Co}^{60}$  with photon energies 1170 and 1330 keV. In Table 4 the Chilton-Huddleston formula used 1250 keV as an equivalent monoenergetic source photon energy.

In Tables 5 and 6 are displayed the  $A_d(\vec{n})$  values corresponding to the  $\alpha_d(\vec{n})$  values in Tables 1 and 2. In Tables 7 through 10 experimental values,  $\alpha_d(\vec{n})$ , are presented for aluminum and steel slabs for selected incident and detection angles. The underlined values are the experimental values. Those values not underlined are calculated from an empirical formula derived in Section IVA.

Table 1  
DOSE ALBEDO,  $\alpha_d(\vec{n})$   
( $\times 10^4$ )

Source: Cs<sup>137</sup>  
Energy: 662 keV

Material: Concrete ( $\rho=155 \text{ lb/ft}^3$ )  
Thickness: 12 in.

$\cos\theta_o = 1.00^*$							
$\phi \backslash \theta$	8°	15°	22°	32°	45°	60°	72°
7.5°	NT**	NT	NT	156	137	102	66
$\cos\theta_o = 0.75$							
	8°	15°	22°	32°	45°	60°	72°
7.5°	221	220	223	229	234	220	182
22.5°	222	221	222	222	220	210	169
37.5°	222	219	220	216	212	190	148
52.5°	220	219	214	210	201	172	127
67.5°	217	213	210	201	189	154	110
82.5°	215	214	208	200	181	142	NT
97.5°	216	209	203	193	NT	NT	NT
112.5°	214	209	NT	NT	NT	NT	NT
127.5°	211	NT	NT	NT	NT	NT	NT
142.5°	212	NT	NT	NT	NT	NT	NT
157.5°	212	NT	NT	NT	NT	NT	NT
172.5°	210	NT	NT	NT	NT	NT	NT
$\cos\theta_o = 0.50$							
	8°	15°	22°	32°	45°	60°	72°
7.5°	297	305	324	356	402	502	516
22.5°	295	302	321	347	370	442	435
37.5°	293	299	306	324	340	362	332
52.5°	291	296	299	304	307	308	236
67.5°	288	290	283	284	272	244	182
82.5°	286	285	268	269	244	206	145
97.5°	280	275	262	256	226	183	126
112.5°	278	269	259	248	213	NT	NT
127.5°	272	268	262	240	NT	NT	NT
142.5°	270	263	259	234	NT	NT	NT
157.5°	265	263	255	228	NT	NT	NT
172.5°	265	258	253	226	NT	NT	NT

\* For normal incidence, albedo is independent of  $\phi$ .

\*\* NT = data not taken because of interference between source and detector or supports.

Table 2  
DOSE ALBEDO,  $\alpha_d(\vec{n})$   
( $\times 10^4$ )

Source:  $\text{Co}^{60}$  Material: Concrete ( $\rho=155 \text{ lb/ft}^3$ )  
Energy: 1170 and 1330 keV Thickness: 12 in.

$\cos\theta_0 = 1.00^*$							
$\phi \backslash \theta$	$8^\circ$	$15^\circ$	$22^\circ$	$32^\circ$	$45^\circ$	$60^\circ$	$72^\circ$
$7.5^\circ$	NT**	NT	NT	99	89	68	42
$\cos\theta_0 = 0.75$							
	$8^\circ$	$15^\circ$	$22^\circ$	$32^\circ$	$45^\circ$	$60^\circ$	$72^\circ$
$7.5^\circ$	151	154	157	164	162	167	145
$22.5^\circ$	151	153	156	161	155	159	128
$37.5^\circ$	149	154	153	155	153	142	111
$52.5^\circ$	146	150	148	148	144	127	93
$67.5^\circ$	146	146	144	140	132	110	79
$82.5^\circ$	144	142	140	134	123	97	NT
$97.5^\circ$	143	139	137	127	NT	NT	NT
$112.5^\circ$	141	137	NT	NT	NT	NT	NT
$127.5^\circ$	141	NT	NT	NT	NT	NT	NT
$142.5^\circ$	140	NT	NT	NT	NT	NT	NT
$157.5^\circ$	141	NT	NT	NT	NT	NT	NT
$172.5^\circ$	139	NT	NT	NT	NT	NT	NT
$\cos\theta_0 = 0.50$							
	$8^\circ$	$15^\circ$	$22^\circ$	$32^\circ$	$45^\circ$	$60^\circ$	$72^\circ$
$7.5^\circ$	219	234	255	289	345	440	480
$22.5^\circ$	215	234	248	280	314	389	393
$37.5^\circ$	214	228	236	255	291	308	297
$52.5^\circ$	211	219	226	234	249	241	207
$67.5^\circ$	204	211	212	214	210	193	143
$82.5^\circ$	198	202	203	188	182	152	109
$97.5^\circ$	193	195	195	175	162	131	88
$112.5^\circ$	194	191	184	167	148	NT	NT
$127.5^\circ$	191	185	179	164	NT	NT	NT
$142.5^\circ$	192	183	172	158	NT	NT	NT
$157.5^\circ$	187	180	174	156	NT	NT	NT
$172.5^\circ$	189	180	171	150	NT	NT	NT

\* For normal incidence, albedo is independent of  $\phi$ .  
\*\* NT = data not taken because of interference between source and detector supports.

Table 3  
CALCULATED DOSE ALBEDO,  $\alpha_d^*$   
( $\times 10^5$ )

Source: Cs<sup>137</sup>  
Energy: 662 keV

Material: Concrete  
Thickness:  $\infty$

$\cos\theta_o = 1.00^{**}$								
$\phi \backslash \theta$	8°	15°	22°	32°	45°	60°	72°	84°
7.5°	1491	1476	1452	1399	1289	1079	804	349
$\cos\theta_o = 0.75$								
	8°	15°	22°	32°	45°	60°	72°	84°
7.5°	1788	1801	1811	1821	1829	1817	1682	980
22.5°	1786	1797	1804	1807	1800	1754	1584	894
37.5°	1782	1789	1790	1782	1749	1652	1431	764
52.5°	1777	1778	1773	1750	1690	1542	1276	640
67.5°	1771	1766	1753	1717	1632	1444	1149	545
82.5°	1764	1753	1733	1686	1582	1367	1056	481
97.5°	1758	1741	1715	1658	1541	1310	993	440
112.5°	1752	1730	1699	1636	1510	1270	950	414
127.5°	1747	1721	1686	1618	1486	1241	923	398
142.5°	1742	1713	1676	1604	1469	1222	905	388
157.5°	1740	1709	1669	1596	1459	1211	894	382
172.5°	1738	1706	1666	1591	1453	1205	889	379
$\cos\theta_o = 0.50$								
	8°	15°	22°	32°	45°	60°	72°	84°
7.5°	2220	2283	2360	2512	2831	3413	3777	2579
22.5°	2215	2271	2337	2463	2711	3123	3295	2145
37.5°	2205	2249	2297	2380	2521	2699	2633	1581
52.5°	2192	2220	2246	2282	2321	2301	2067	1135
67.5°	2177	2188	2193	2189	2150	2005	1684	858
82.5°	2162	2157	2144	2108	2020	1808	1455	704
97.5°	2146	2128	2101	2044	1927	1684	1322	621
112.5°	2132	2102	2065	1995	1862	1606	1245	576
127.5°	2120	2082	2038	1959	1818	1556	1199	550
142.5°	2111	2067	2018	1934	1788	1525	1171	535
157.5°	2105	2057	2004	1918	1770	1506	1154	527
172.5°	2102	2051	1998	1910	1761	1498	1147	523

\* Monte Carlo calculations of Raso interpolated by Chilton-Huddleston semi-empirical formula with  $C = 0.0390$  and  $C' = 0.0170$ .

\*\* For normal incidence, albedo is independent of  $\phi$ .

Table 4

CALCULATED DOSE ALBEDO,  $\alpha_d^*$   
( $\times 10^5$ )Source:  $\text{Co}^{60}$   
Energy: 1250 keVMaterial: Concrete  
Thickness:  $\infty$ 

$\cos \theta_o = 1.00^{**}$								
$\phi \backslash \theta$	$8^\circ$	$15^\circ$	$22^\circ$	$32^\circ$	$45^\circ$	$60^\circ$	$72^\circ$	$84^\circ$
$7.5^\circ$	833	827	818	796	749	648	500	227
$\cos \theta_o = 0.75$								
	$8^\circ$	$15^\circ$	$22^\circ$	$32^\circ$	$45^\circ$	$60^\circ$	$72^\circ$	$84^\circ$
$7.5^\circ$	1047	1072	1098	1138	1197	1264	1240	782
$22.5^\circ$	1045	1067	1090	1124	1170	1209	1151	696
$37.5^\circ$	1041	1059	1076	1098	1122	1118	1016	574
$52.5^\circ$	1035	1047	1057	1066	1065	1018	879	462
$67.5^\circ$	1028	1033	1035	1031	1008	927	765	377
$82.5^\circ$	1021	1019	1013	997	956	852	679	320
$97.5^\circ$	1014	1005	993	967	912	794	617	282
$112.5^\circ$	1007	993	975	941	876	751	574	256
$127.5^\circ$	1001	982	960	920	850	719	543	240
$142.5^\circ$	996	973	948	905	830	697	523	229
$157.5^\circ$	993	968	940	895	818	684	511	222
$172.5^\circ$	991	965	936	890	812	677	505	219
$\cos \theta_o = 0.50$								
	$8^\circ$	$15^\circ$	$22^\circ$	$32^\circ$	$45^\circ$	$60^\circ$	$72^\circ$	$84^\circ$
$7.5^\circ$	1364	1434	1520	1681	2001	2615	3196	2538
$22.5^\circ$	1359	1422	1498	1637	1896	2344	2680	1961
$37.5^\circ$	1349	1400	1459	1560	1728	1959	2022	1307
$52.5^\circ$	1336	1372	1410	1469	1549	1607	1501	862
$67.5^\circ$	1320	1339	1357	1379	1392	1343	1163	610
$82.5^\circ$	1303	1306	1306	1298	1266	1162	956	474
$97.5^\circ$	1287	1275	1261	1231	1171	1040	831	398
$112.5^\circ$	1272	1248	1222	1179	1102	958	752	354
$127.5^\circ$	1259	1226	1192	1138	1053	904	702	326
$142.5^\circ$	1249	1209	1169	1110	1019	868	670	309
$157.5^\circ$	1242	1198	1154	1092	998	847	651	300
$172.5^\circ$	1238	1192	1147	1083	988	836	642	295

\* Monte Carlo calculations of Raso interpolated by Chilton-Huddleston semi-empirical formula with  $C = 0.0630$  and  $C' = 0.0093$ .

\*\* For normal incidence, albedo is independent of  $\phi$ .

Table 5  
DOSE-RATE RATIO,  $A_d(\vec{n})$   
( $\times 10^4$ )

Source:  $\text{Cs}^{137}$   
Energy: 662 keV

Material: Concrete ( $\rho=155 \text{ lb/ft}^3$ )  
Thickness: 12 in.

$\cos\theta_o = 1.00^*$							
$\phi \backslash \theta$	$8^\circ$	$15^\circ$	$22^\circ$	$32^\circ$	$45^\circ$	$60^\circ$	$72^\circ$
$7.5^\circ$	NT**	NT	NT	184	193	204	213
$\cos\theta_o = 0.75$							
	$8^\circ$	$15^\circ$	$22^\circ$	$32^\circ$	$45^\circ$	$60^\circ$	$72^\circ$
$7.5^\circ$	168	171	181	202	249	330	441
$22.5^\circ$	168	171	180	197	233	314	411
$37.5^\circ$	168	170	178	191	225	284	359
$52.5^\circ$	166	170	174	186	213	258	307
$67.5^\circ$	164	167	170	178	200	231	267
$82.5^\circ$	163	166	168	177	193	213	NT
$97.5^\circ$	164	163	164	171	NT	NT	NT
$112.5^\circ$	162	163	NT	NT	NT	NT	NT
$127.5^\circ$	160	NT	NT	NT	NT	NT	NT
$142.5^\circ$	161	NT	NT	NT	NT	NT	NT
$157.5^\circ$	161	NT	NT	NT	NT	NT	NT
$172.5^\circ$	159	NT	NT	NT	NT	NT	NT
$\cos\theta_o = 0.50$							
	$8^\circ$	$15^\circ$	$22^\circ$	$32^\circ$	$45^\circ$	$60^\circ$	$72^\circ$
$7.5^\circ$	150	158	175	210	284	502	835
$22.5^\circ$	149	156	173	204	262	442	703
$37.5^\circ$	148	155	165	191	240	362	537
$52.5^\circ$	147	153	161	179	217	308	382
$67.5^\circ$	145	150	152	167	193	244	294
$82.5^\circ$	144	147	145	159	173	206	235
$97.5^\circ$	142	142	141	151	160	183	204
$112.5^\circ$	141	139	140	146	150	NT	NT
$127.5^\circ$	138	139	141	142	144	NT	NT
$142.5^\circ$	136	136	140	138	NT	NT	NT
$157.5^\circ$	134	136	138	134	NT	NT	NT
$172.5^\circ$	134	135	136	133	NT	NT	NT

\* For normal incidence, albedo is independent of  $\phi$ .

\*\* NT = data not taken because of interference between source and detector supports.

Table 6  
DOSE-RATE RATIO,  $A_d(\vec{n})$   
( $\times 10^4$ )

Source:  $\text{Co}^{60}$  Material: Concrete ( $\rho=155 \text{ lb/ft}^3$ )  
Energy: 1170 and 1330 keV Thickness: 12 in.

$\cos\theta_0 = 1.00^*$							
$\phi \backslash \theta$	$8^\circ$	$15^\circ$	$22^\circ$	$32^\circ$	$45^\circ$	$60^\circ$	$72^\circ$
$7.5^\circ$	NT**	NT	NT	117	126	136	137
$\cos\theta_0 = 0.75$							
	$8^\circ$	$15^\circ$	$22^\circ$	$32^\circ$	$45^\circ$	$60^\circ$	$72^\circ$
$7.5^\circ$	114	120	127	145	172	251	351
$22.5^\circ$	114	119	126	143	165	238	312
$37.5^\circ$	113	119	124	137	162	213	271
$52.5^\circ$	110	116	120	131	153	190	225
$67.5^\circ$	111	113	116	124	140	165	191
$82.5^\circ$	109	111	113	119	130	146	NT
$97.5^\circ$	109	108	111	113	NT	NT	NT
$112.5^\circ$	107	107	NT	NT	NT	NT	NT
$127.5^\circ$	107	NT	NT	NT	NT	NT	NT
$142.5^\circ$	106	NT	NT	NT	NT	NT	NT
$157.5^\circ$	106	NT	NT	NT	NT	NT	NT
$172.5^\circ$	105	NT	NT	NT	NT	NT	NT
$\cos\theta_0 = 0.50$							
	$8^\circ$	$15^\circ$	$22^\circ$	$32^\circ$	$45^\circ$	$60^\circ$	$72^\circ$
$7.5^\circ$	111	121	137	170	244	440	776
$22.5^\circ$	109	121	134	165	222	389	637
$37.5^\circ$	108	118	127	150	206	308	481
$52.5^\circ$	106	114	122	138	176	241	335
$67.5^\circ$	103	109	115	126	148	193	231
$82.5^\circ$	100	105	110	111	129	152	176
$97.5^\circ$	98	101	105	103	115	131	142
$112.5^\circ$	98	99	99	98	104	NT	NT
$127.5^\circ$	96	96	96	97	NT	NT	NT
$142.5^\circ$	96	94	93	93	NT	NT	NT
$157.5^\circ$	94	93	94	92	NT	NT	NT
$172.5^\circ$	95	93	92	89	NT	NT	NT

\* For normal incidence, albedo is independent of  $\phi$ .

\*\* NT = data not taken because of interference between source and detector supports.



Table 7

DOSE ALBEDO,  $\alpha_d(\vec{n})$   
( $\times 10^4$ )

(underlined values are experimental values)

Source: Cs<sup>137</sup>

Material: Aluminum

Energy: 662 keV

Thickness: 12 in.

$\cos\theta_0 = 1.00$ *							
$\phi \backslash \theta$	8°	15°	22°	32°	45°	60°	72°
7.5°	185	181	175	162	<u>137</u>	101	<u>65</u>
$\cos\theta_0 = 0.75$							
	8°	15°	22°	32°	45°	60°	72°
7.5°	235	<u>227</u>	225	<u>231</u>	226	<u>221</u>	<u>190</u>
22.5°	<u>235</u>	<u>227</u>	224	<u>227</u>	<u>221</u>	<u>211</u>	<u>178</u>
37.5°	<u>234</u>	225	223	223	<u>212</u>	196	155
52.5°	232	224	220	219	201	179	132
67.5°	232	223	<u>217</u>	215	191	163	116
82.5°	231	220	<u>215</u>	210	186	152	103
97.5°	231	219	211	207	181	145	95
112.5°	231	219	211	205	177	141	91
127.5°	231	219	211	205	176	138	89
142.5°	231	218	210	202	174	138	87
157.5°	231	218	209	200	173	137	87
172.5°	231	216	208	199	172	136	87
$\cos\theta_0 = 0.50$							
	8°	15°	22°	32°	45°	60°	72°
7.5°	<u>297</u>	<u>308</u>	302	346	413	485	<u>509</u>
22.5°	<u>295</u>	<u>305</u>	299	332	<u>380</u>	<u>422</u>	<u>421</u>
37.5°	293	299	284	<u>312</u>	<u>335</u>	333	305
52.5°	293	292	273	<u>287</u>	293	254	211
67.5°	289	286	260	265	252	198	150
82.5°	287	280	248	246	223	160	115
97.5°	285	276	243	236	206	137	95
112.5°	281	272	<u>236</u>	227	197	128	86
127.5°	279	269	<u>232</u>	220	191	121	82
142.5°	277	265	228	219	190	119	80
157.5°	277	263	226	217	187	117	78
172.5°	277	261	226	217	184	115	77

\* For normal incidence, albedo is independent of  $\phi$ .

Table 8

DOSE ALBEDO,  $\alpha_a(\vec{n})$   
( $\times 10^4$ )Source:  $\text{Co}^{60}$  (underlined values are experimental values)

Material: Aluminum

Energy: 1170 and 1330 keV

Thickness: 12 in.

$\cos\theta_o = 1.00^*$							
$\phi \backslash \theta$	$8^\circ$	$15^\circ$	$22^\circ$	$32^\circ$	$45^\circ$	$60^\circ$	$72^\circ$
$7.5^\circ$	109	106	104	<u>97</u>	82	62	42
$\cos\theta_o = 0.75$							
	$8^\circ$	$15^\circ$	$22^\circ$	$32^\circ$	$45^\circ$	$60^\circ$	$72^\circ$
$7.5^\circ$	144	<u>155</u>	152	<u>163</u>	178	<u>171</u>	146
$22.5^\circ$	<u>144</u>	<u>155</u>	151	<u>159</u>	<u>172</u>	<u>161</u>	<u>134</u>
$37.5^\circ$	<u>143</u>	153	150	155	<u>164</u>	145	108
$52.5^\circ$	141	152	147	152	153	128	89
$67.5^\circ$	141	151	<u>145</u>	147	143	113	72
$82.5^\circ$	140	148	<u>142</u>	142	138	101	60
$97.5^\circ$	140	147	138	139	133	95	52
$112.5^\circ$	140	147	138	137	129	91	47
$127.5^\circ$	140	147	138	137	128	87	45
$142.5^\circ$	140	146	137	135	126	87	43
$157.5^\circ$	140	146	136	132	124	86	43
$172.5^\circ$	140	144	135	131	124	85	43
$\cos\theta_o = 0.50$							
	$8^\circ$	$15^\circ$	$22^\circ$	$32^\circ$	$45^\circ$	$60^\circ$	$72^\circ$
$7.5^\circ$	<u>216</u>	<u>232</u>	250	282	342	450	476
$22.5^\circ$	<u>214</u>	<u>230</u>	247	268	310	<u>388</u>	<u>388</u>
$37.5^\circ$	212	224	232	<u>248</u>	<u>264</u>	299	272
$52.5^\circ$	212	216	221	<u>222</u>	222	220	179
$67.5^\circ$	208	211	208	200	181	164	117
$82.5^\circ$	206	205	197	181	153	126	82
$97.5^\circ$	204	201	191	171	136	103	62
$112.5^\circ$	200	195	<u>183</u>	163	126	94	53
$127.5^\circ$	198	193	<u>180</u>	156	120	87	49
$142.5^\circ$	196	189	176	154	119	85	47
$157.5^\circ$	196	187	174	153	116	83	46
$172.5^\circ$	196	185	174	153	113	81	44

\* For normal incidence, albedo is independent of  $\phi$ .

Table 9  
DOSE ALBEDO,  $\alpha_d(\vec{n})$   
( $\times 10^4$ )

(underlined values are experimental values)

Source:  $\text{Cs}^{137}$   
Energy: 662 keV

Material: Steel  
Thickness: 5.5 in.

$\cos\theta_0 = 1.00^*$							
$\phi \backslash \theta$	$8^\circ$	$15^\circ$	$22^\circ$	$32^\circ$	$45^\circ$	$60^\circ$	$72^\circ$
$7.5^\circ$	135	131	128	<u>110</u>	<u>98</u>	<u>81</u>	50
$\cos\theta_0 = 0.75$							
	$8^\circ$	$15^\circ$	$22^\circ$	$32^\circ$	$45^\circ$	$60^\circ$	$72^\circ$
$7.5^\circ$	<u>166</u>	<u>170</u>	164	162	185	189	<u>171</u>
$22.5^\circ$	<u>166</u>	<u>170</u>	163	158	<u>180</u>	179	<u>159</u>
$37.5^\circ$	165	169	162	154	<u>171</u>	<u>163</u>	136
$52.5^\circ$	164	167	159	150	159	<u>146</u>	114
$67.5^\circ$	164	166	157	146	150	131	97
$82.5^\circ$	162	164	155	141	144	119	85
$97.5^\circ$	162	162	151	138	140	113	77
$112.5^\circ$	162	162	<u>150</u>	136	136	109	73
$127.5^\circ$	162	162	<u>150</u>	136	135	105	70
$142.5^\circ$	162	161	150	<u>133</u>	133	105	68
$157.5^\circ$	162	161	148	<u>131</u>	131	104	68
$172.5^\circ$	162	160	147	130	130	103	68
$\cos\theta_0 = 0.50$							
	$8^\circ$	$15^\circ$	$22^\circ$	$32^\circ$	$45^\circ$	$60^\circ$	$72^\circ$
$7.5^\circ$	<u>224</u>	<u>240</u>	261	299	345	471	<u>461</u>
$22.5^\circ$	<u>222</u>	<u>238</u>	258	285	<u>312</u>	408	<u>375</u>
$37.5^\circ$	220	232	243	265	<u>267</u>	<u>319</u>	258
$52.5^\circ$	220	224	232	239	225	<u>240</u>	164
$67.5^\circ$	216	218	219	217	183	184	103
$82.5^\circ$	212	213	208	198	156	146	68
$97.5^\circ$	210	209	202	188	139	123	48
$112.5^\circ$	208	203	<u>194</u>	180	129	114	39
$127.5^\circ$	206	201	<u>191</u>	173	123	107	35
$142.5^\circ$	204	197	187	<u>172</u>	122	105	33
$157.5^\circ$	204	195	185	<u>170</u>	119	103	32
$172.5^\circ$	204	193	185	170	116	101	30

\* For normal incidence, albedo is independent of  $\phi$ .

Table 10  
DOSE ALBEDO,  $\alpha_d(\vec{n})$   
( $\times 10^4$ )

(underlined values are experimental values)

Source:  $\text{Co}^{60}$

Energy: 1170 and 1330 keV

Material: Steel

Thickness: 5.5 in.

$\cos\theta_0 = 1.00$ *							
$\phi \backslash \theta$	$8^\circ$	$15^\circ$	$22^\circ$	$32^\circ$	$45^\circ$	$60^\circ$	$72^\circ$
$7.5^\circ$	78	76	75	<u>67</u>	<u>58</u>	<u>47</u>	<u>32</u>
$\cos\theta_0 = 0.75$							
	$8^\circ$	$15^\circ$	$22^\circ$	$32^\circ$	$45^\circ$	$60^\circ$	$72^\circ$
$7.5^\circ$	<u>120</u>	<u>125</u>	117	122	145	159	<u>148</u>
$22.5^\circ$	<u>120</u>	<u>125</u>	116	119	<u>139</u>	149	<u>136</u>
$37.5^\circ$	119	124	115	114	<u>131</u>	<u>134</u>	113
$52.5^\circ$	118	122	112	111	120	<u>117</u>	91
$67.5^\circ$	118	121	110	106	110	101	74
$82.5^\circ$	116	118	108	102	105	90	62
$97.5^\circ$	116	117	104	98	100	83	54
$112.5^\circ$	116	117	<u>104</u>	96	96	79	49
$127.5^\circ$	116	117	<u>104</u>	96	95	76	47
$142.5^\circ$	116	116	103	94	93	76	45
$157.5^\circ$	116	116	101	92	91	75	45
$172.5^\circ$	116	115	100	90	91	74	45
$\cos\theta_0 = 0.50$							
	$8^\circ$	$15^\circ$	$22^\circ$	$32^\circ$	$45^\circ$	$60^\circ$	$72^\circ$
$7.5^\circ$	191	<u>206</u>	224	258	318	445	<u>458</u>
$22.5^\circ$	<u>188</u>	<u>205</u>	221	244	<u>286</u>	383	<u>370</u>
$37.5^\circ$	186	199	206	224	<u>240</u>	<u>294</u>	254
$52.5^\circ$	186	191	195	198	198	<u>215</u>	161
$67.5^\circ$	182	185	182	176	157	159	100
$82.5^\circ$	180	180	171	158	129	121	64
$97.5^\circ$	178	178	165	148	112	98	44
$112.5^\circ$	174	170	<u>158</u>	139	102	89	35
$127.5^\circ$	172	168	<u>154</u>	132	96	82	<u>31</u>
$142.5^\circ$	170	164	150	<u>130</u>	95	80	29
$157.5^\circ$	170	162	148	<u>130</u>	92	78	28
$172.5^\circ$	170	160	148	130	89	76	27

\* For normal incidence, albedo is independent of  $\phi$ .

#### IV. DATA ANALYSIS

##### A. Concrete

Since a model of albedo has been suggested<sup>5</sup> which utilizes single Compton scattering as one of the important processes, it seemed natural to attempt to plot the experimental data as a function  $\theta_s$ .  $\theta_s$  is the angle appearing in the Compton formula

$$\lambda = \lambda_o = \frac{h}{mc} (1 - \cos\theta_s).$$

From Fig. 1 it may be seen that  $\theta_s$  is related to  $\theta_o$ ,  $\theta$ , and  $\phi$  by the following formula:

$$\cos\theta_s = \sin\theta_o \sin\theta \cos\phi - \cos\theta_o \cos\theta.$$

Various plots of the data in terms of  $\alpha_d(\vec{\Omega})$  and  $A_d(\vec{\Omega})$  versus  $\theta_s$  and  $\cos\theta_s$  were tried. It was found that, when  $A_d(\vec{\Omega})$  was plotted versus  $\theta_s$ , all of the points for the same source energy,  $h\nu_o$ , and incidence angle,  $\theta_o$ , fell near a single smooth curve.

Further investigation yielded an empirical formula for these curves:

$$A_d(\vec{\Omega}) = c e^{-m\theta_s} + b. \quad (1)$$

Since the form of this equation was suggested by a similar dependence upon scattering angle of transmitted angular dose\* for  $\phi = 0$  the parameters c, m and b were evaluated for each  $(h\nu_0, \theta_0)$  set by fitting these points for which  $\phi = 7.5$  deg.

In Table 11 the values found for these parameters are shown. The solid curve in each of Figs. 2-5 has been calculated using formula (1) and the appropriate parametric values from Table 11.

Table 11  
EMPIRICAL-FIT PARAMETERS  
TO EXPERIMENTAL  $A_d$  VALUES FOR CONCRETE

$\cos \theta_0$		c	m	b
Cs <sup>137</sup>	1.00	.102	1.660	.0171
	.75	.330	2.131	.0142
	.50	1.260	3.362	.0133
Co <sup>60</sup>	1.00	.202	1.970	.0105
	.75	.461	2.482	.0098
	.50	.739	2.892	.0085

The exponential variation with  $\theta_s$  is most strikingly demonstrated by plotting  $[A_d(\bar{n}) - b]$  versus  $\theta_s$  in radians (Figs. 6-9). In each of these figures the b level, which has been subtracted, is indicated as a dashed line. From our experiences with the dosimetry system we attribute the scattering of points around the  $e^{-m\theta_s}$  line to instrumental instability rather than to physical relationships.

\* Unpublished investigation by N. E. Scofield.

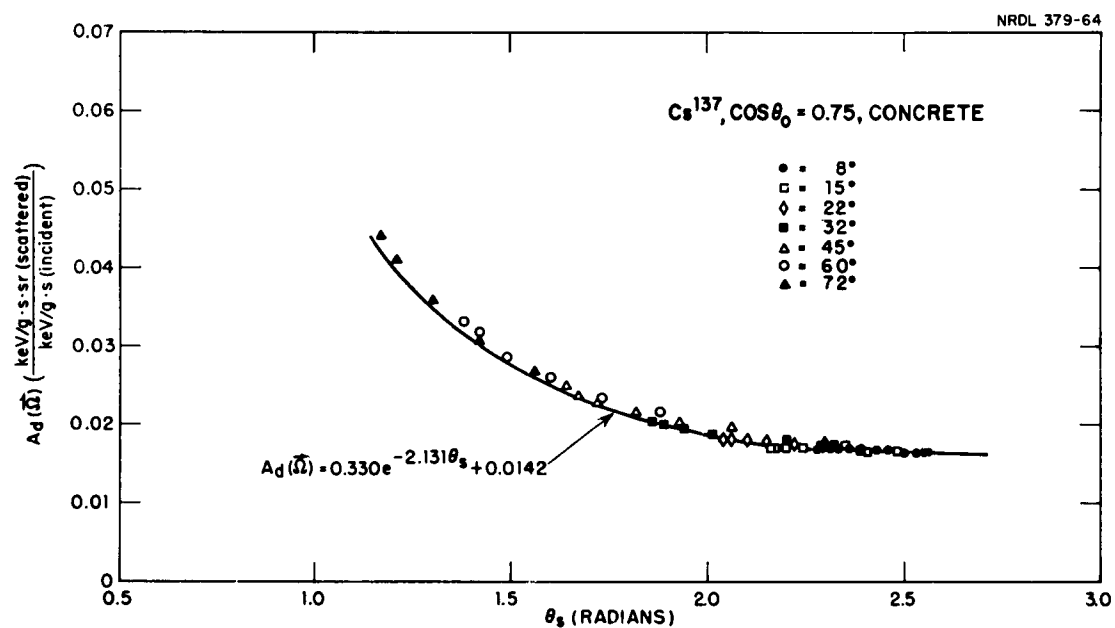


Fig. 2  $A_d(\vec{\Omega})$  vs.  $\theta_s$ . The experimental data are plotted with symbols corresponding to the  $\theta$  angles at which they were taken.

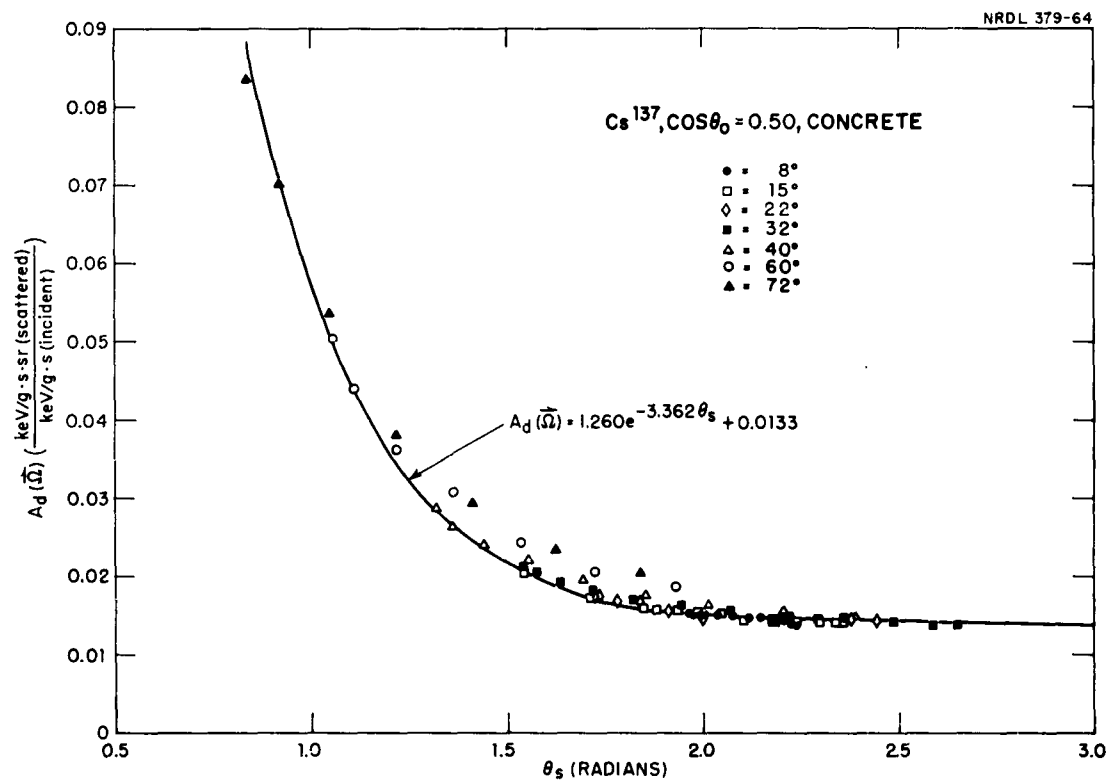


Fig. 3  $A_d(\vec{n})$  vs.  $\theta_s$ . The experimental data are plotted with symbols corresponding to the  $\theta$  angles at which they were taken.



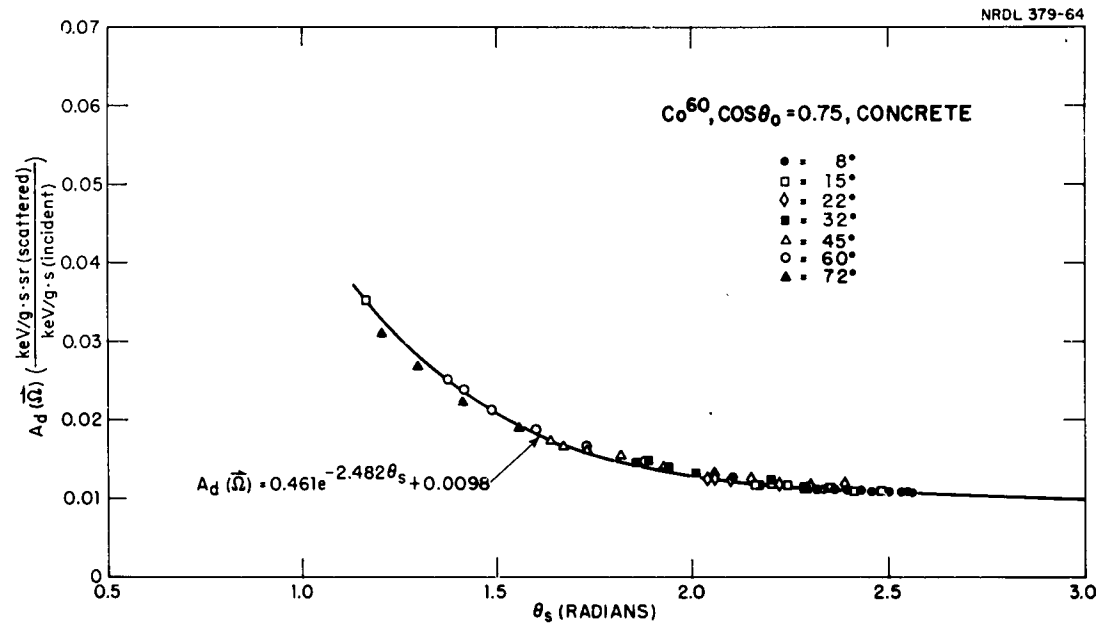


Fig. 4  $A_d(\vec{\Omega})$  vs.  $\theta_s$ . The experimental data are plotted with symbols corresponding to the  $\theta$  angles at which they were taken.

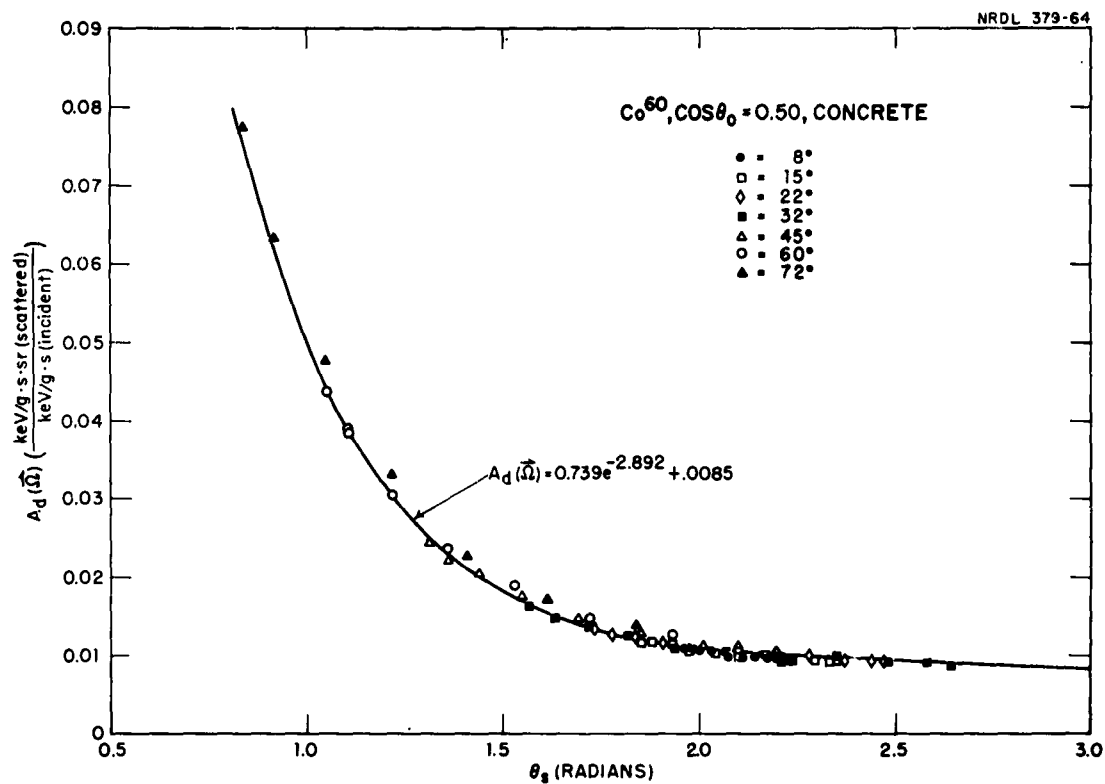


Fig. 5  $A_d(\vec{\Omega})$  vs.  $\theta_s$ . The experimental data are plotted with symbols corresponding to the  $\theta$  angles at which they were taken.

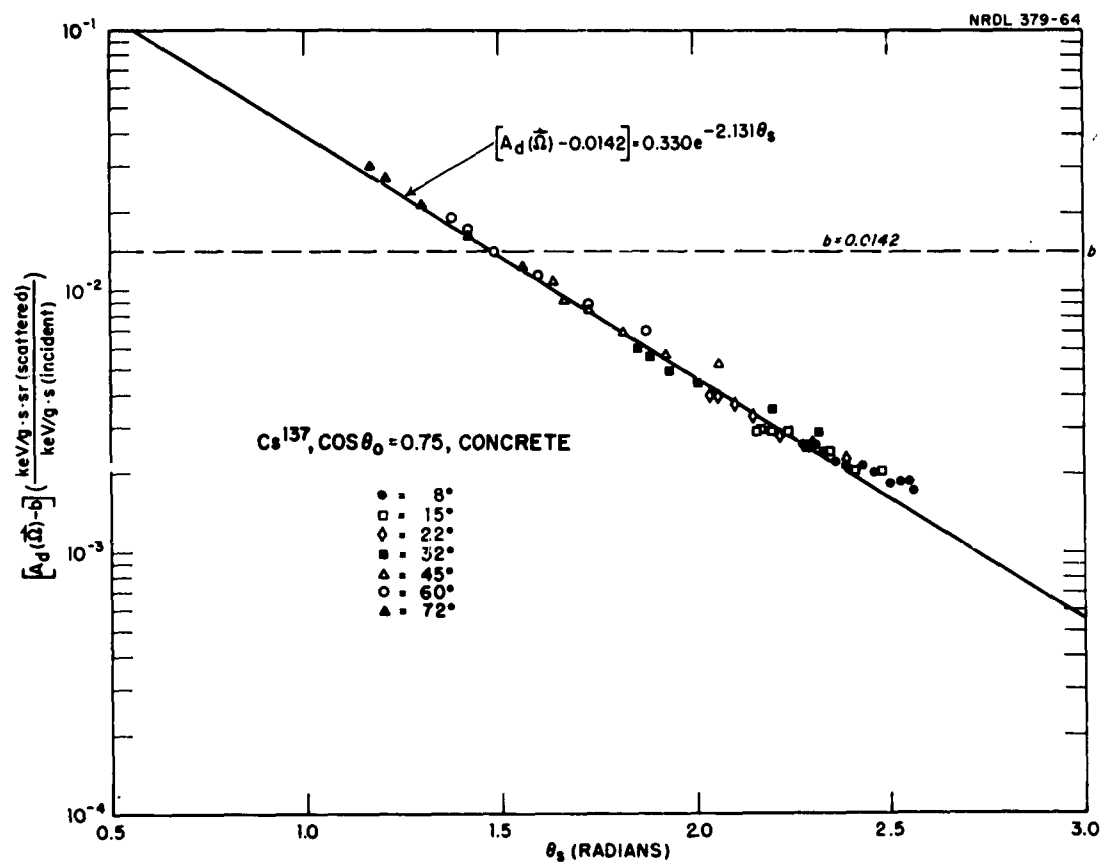


Fig. 6  $[A_d(\hat{\Omega}) - b]$  vs.  $\theta_s$ . The experimental data are plotted with symbols corresponding to the  $\theta$  angles at which they were taken.

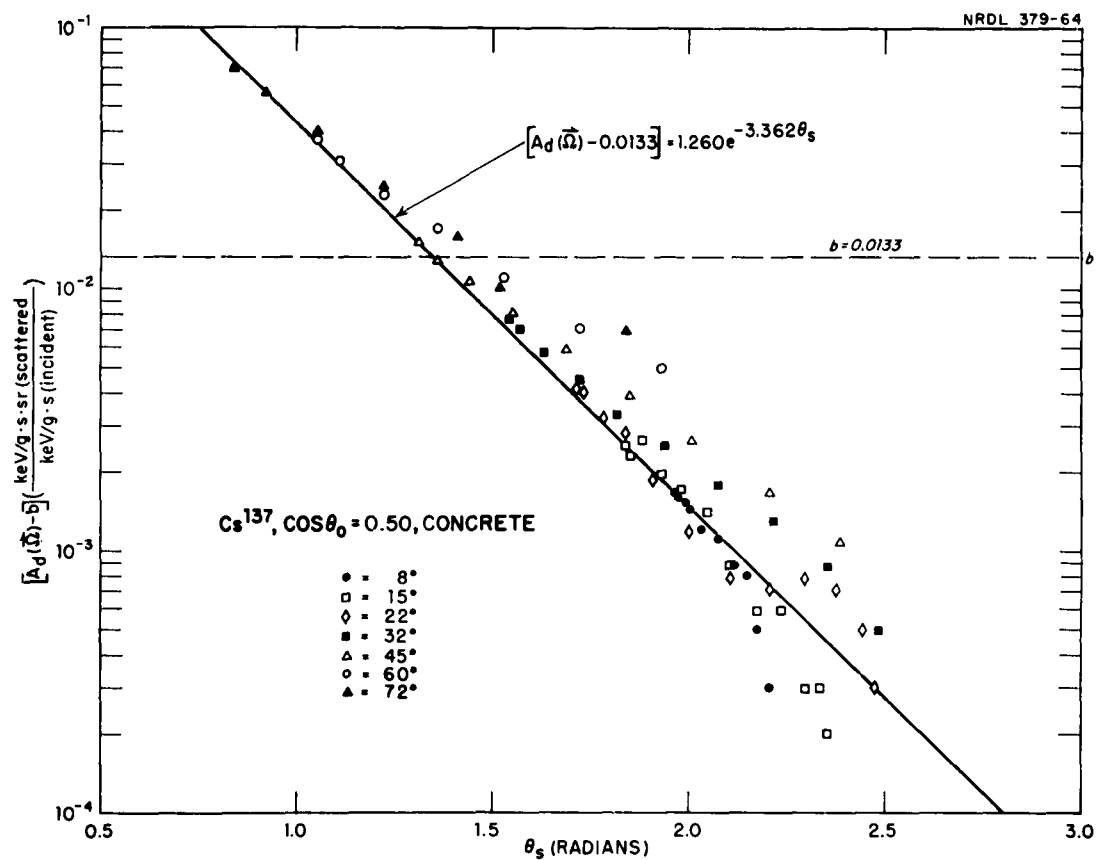


Fig. 7  $[A_d(\vec{\Omega}) - b]$  vs.  $\theta_s$ . The experimental data are plotted with symbols corresponding to the  $\theta$  angles at which they were taken.

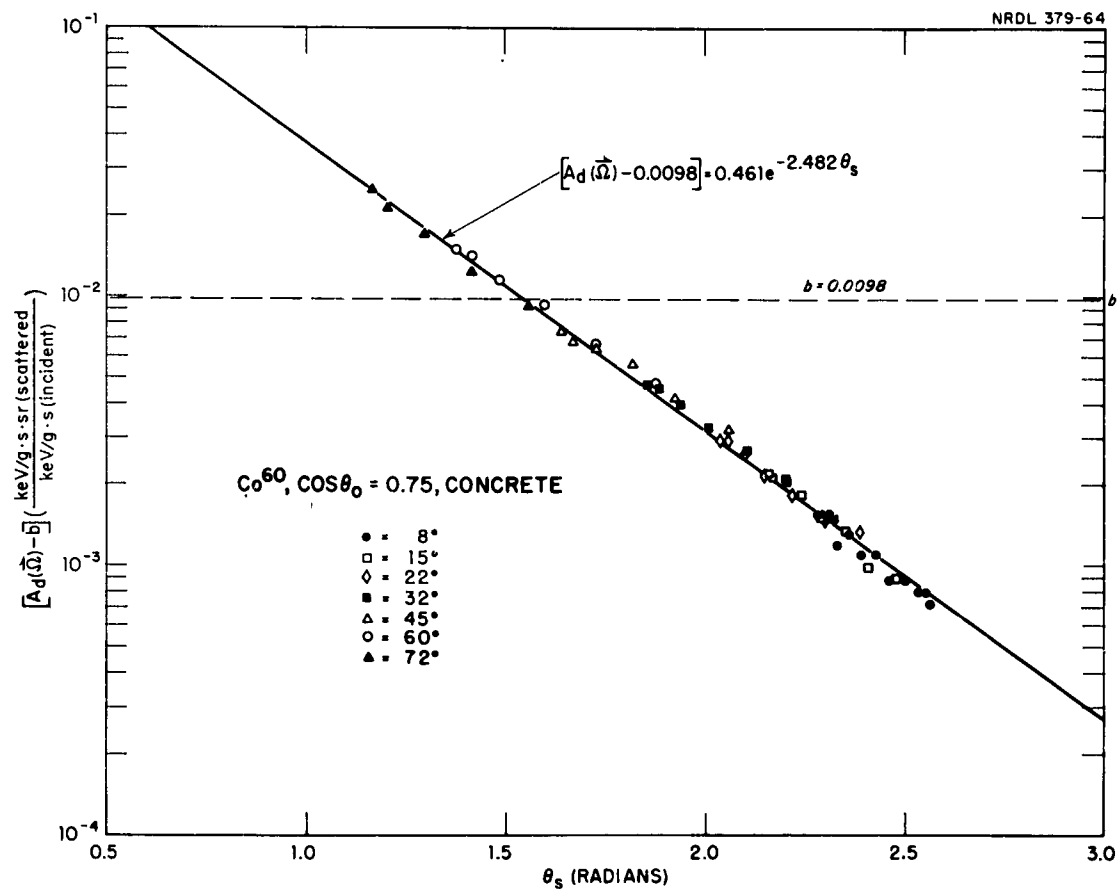


Fig. 8  $[A_d(\vec{\Omega}) - b]$  vs.  $\theta_s$ . The experimental data are plotted with symbols corresponding to the  $\theta$  angles at which they were taken.

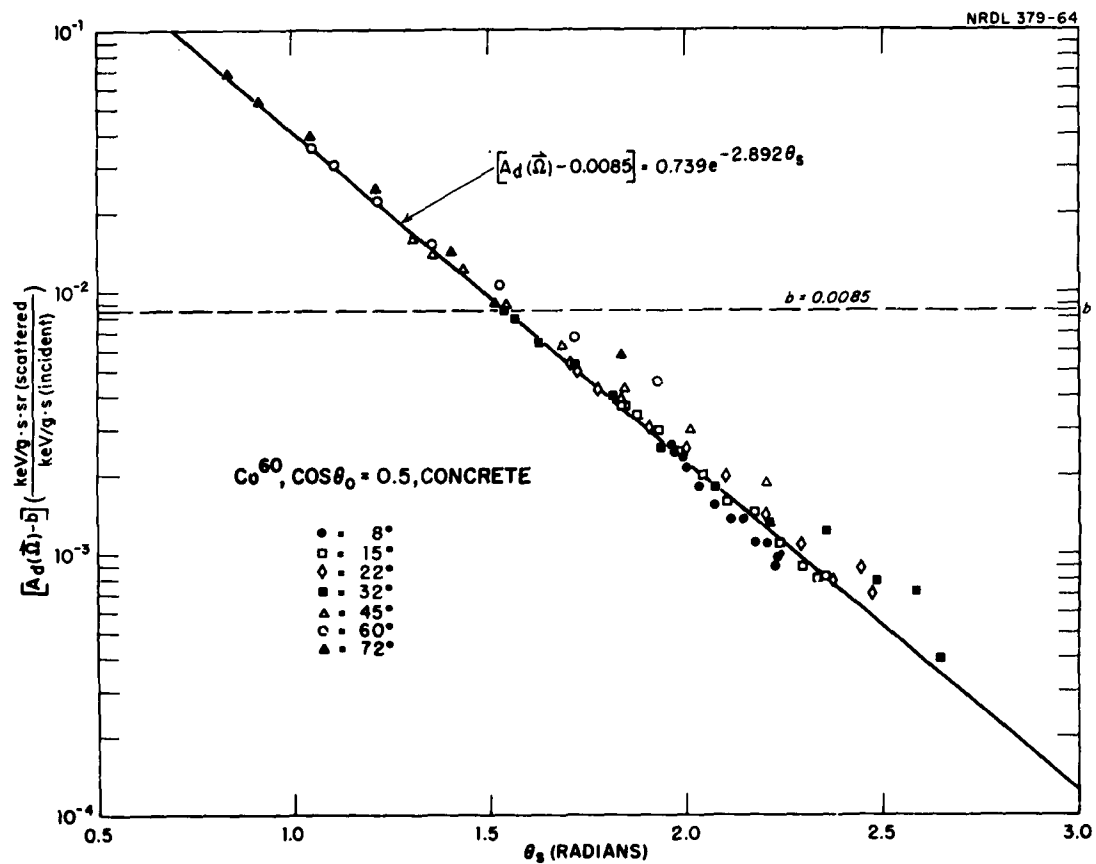


Fig. 9  $[A_d(\hat{\Omega})-b]$  vs.  $\theta_s$ . The experimental data are plotted with symbols corresponding to the  $\theta$  angles at which they were taken.

## B. Aluminum and Steel

Measurements using concrete as the scattering medium were completed and analyzed prior to any measurements using aluminum or steel. Thus the empirical relationship between the scattering angle and dose-rate ratio had already been noted and the necessity for measurements at more than representative space-angle ( $\theta_s$ ) positions was obviated. The positions selected were those for which underlined values of  $\alpha_d(\vec{n})$  appear in Tables 7 through 10.

In the process of deriving the c, m and b parameters for these aluminum and steel data it was observed that the shape of their curves approximated those of any set of concrete data points. This suggested that, if suitable average values  $\bar{c}$  and  $\bar{m}$  were selected, all of the dose albedo data points taken could be fit by a single-parameter formula:

$$\overline{A_d(\vec{n})} = \bar{c} e^{-\bar{m}\theta_s} + b$$

where now only b is a function of  $E$ ,  $\theta$  and  $Z$ . This simplification is, necessarily, accompanied by some loss in accuracy. In Fig. 10 the differences,  $[A_d(\vec{n}) - b]$ , between the measured dose-albedo values and the fitting parameter, b, are plotted as points and the function,  $e^{-\pi\theta_s}$ , is drawn as a solid curve. The empirically determined values of b for each  $(E_0, \theta_0, Z)$  configuration are tabulated in the figure. The selection of 1 for  $\bar{c}$  and  $\pi$  for  $\bar{m}$  was made by an approximation process. No fundamental significance is to be inferred from their presence in the formula since they were chosen partly for their mnemonic value.

Although no extensive effort was made to optimize the fit, 90 percent of the data points,  $A_d(\vec{n})$ , fall within 15 percent of the value,  $\overline{A_d(\vec{n})}$ , predicted by the formula for the same angle,  $\theta_s$ .

Thus the values of  $\alpha_d(\vec{n})$  in Tables 7 through 10 not experimentally measured have been calculated by the formula:

$$\alpha_d(\vec{n}) = \frac{\cos\theta}{\cos\theta_0} \left[ e^{-\pi\theta_s} + b \right]$$

where the values of b for each combination of source, scattering medium,  $\theta_0$ , and  $\theta$  were determined from the experimentally measured value for that combination.

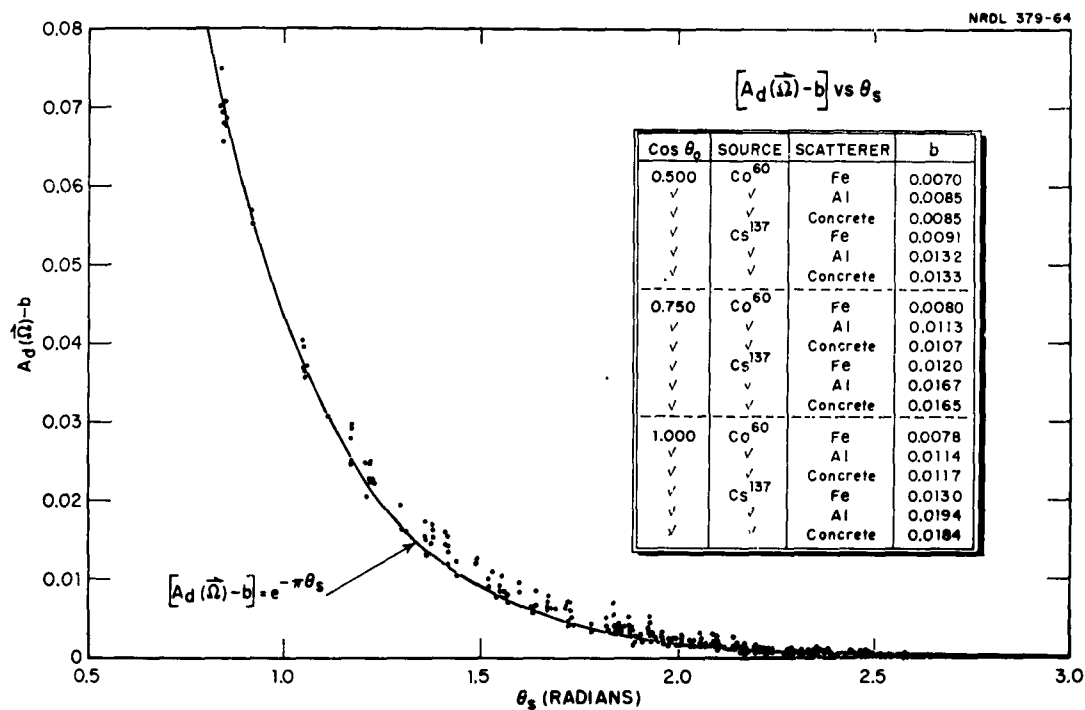


Fig. 10  $[A_d(\vec{\Omega})-b]$  vs.  $\theta_s$ . The b values in the legend were subtracted from the appropriate  $A_d(\vec{\Omega})$  values. The  $A_d(\vec{\Omega})$  values for concrete are in Tables 5 and 6. For aluminum and steel, the  $\alpha_d(\vec{\Omega})$  values underlined in Tables 7 through 10 were converted to  $A_d(\vec{\Omega})$ .



## V. ERROR ESTIMATION AND DISCUSSION OF RESULTS

### A. Systematic Error

The probable systematic error in albedo depends in part on the probable error in the experimental  $(I_d)_0$ 's. The strength of the sources was determined by measuring the dose rate at various distances from the sources using calibrated Landsverk and Baldwin-Farmer dosimeters. These measurements had a probable error of 0.3 percent, but it is unlikely that the source strengths were known on an absolute basis to better than 2 percent. An even greater source of systematic error is in  $K_s$ , the system dose conversion factor. The method of finding  $K_s$  and its probable error is described in Appendix II, D. The probable error of 1.4 percent refers only to  $K(h\nu, T)_1$  for 123.5 keV to 662 keV photons. The degree to which the reductor formula predicts dose for photons outside of this energy region is not known. However, from previous spectral measurements<sup>1</sup> for space angles up to  $\theta_s = 60^\circ$ , it is known that the photon number flux density for scattered radiation falls off rapidly for photon energies below 100 keV; further, all scattered photons from Cs<sup>137</sup> and most scattered from Co<sup>60</sup> for the experimental  $\theta_s$  values have energies less than 662 keV. Thus, even if  $K(h\nu, T)$  should vary considerably from the observed trend, we estimate the overall probable systematic error to be no greater than 10 percent.

### B. Relative Error

Many dose-rate measurements were repeated during the course of the experiment. The repetitions were made after various combinations of source and detector repositioning and gain adjustment after equipment breakdown or time lapse. The measurements were found to be reproducible to within 1 percent. However, if one considers the scatter of data points in the  $A_d(\bar{n})$  versus  $\theta_0$  presentations of Figs. 2-5 to be a measure of relative error, it is seen to be on the order of 5 percent.

### C. Discussion and Comparisons

Comparisons have been made between the empirical curve of Fig. 3, found for the experimental  $A_d(\bar{n})$  values of Cs<sup>137</sup>, concrete,

$\cos\theta_0 = 0.50$ , and the values of Clifford<sup>6</sup> and of Chilton-Huddleston. In Fig. 11 the data of Clifford are represented by point symbols corresponding to particular values of  $\theta$ . It may be seen that, though the scatter of data points is large, the data are not inconsistent with the empirical curve. The  $Q_1$  values of Chilton-Huddleston were converted to  $A_1$  and are shown in Fig. 12 together with the empirical curve. Here values derived from the C-H formula vary smoothly with  $\theta$ , but there appear to be systematic variations with both  $\theta$  and  $\theta_0$  from the experimentally based curve.

The latter conclusions were verified when a point by point comparison was made by calculating the ratio of the NRDL data, presented in Tables 1 and 2, to the C-H formula values using the Raso parameters, presented in Tables 3 and 4. It was found that agreement is less than satisfactory. The difference between theory and experiment is rarely less than 20 percent as shown by the histogram for Cs<sup>137</sup> in Fig. 13 and frequently exceeds 50 percent as shown by the histogram for Co<sup>60</sup> in the same figure.

The original Monte Carlo calculations of Raso for concrete dose albedo have been redone following discovery of an error in the program. Chilton-Huddleston have derived new values for the parameters in their semi-empirical formula based on the revised data of Raso. The new values for Cs<sup>137</sup> are:  $G = 0.0404 \pm 0.0020$ ,  $G' = 0.0172 \pm 0.0012$ ; and for Co<sup>60</sup> are  $G = 0.0645 \pm 0.0022$ ,  $G' = 0.0090 \pm 0.0007$ .<sup>\*</sup> No tabulation of the  $Q_1$  values, based on these new parametric values, was available at the time this report was compiled. Therefore, the  $Q_1$  values, based on the original parametric values noted in Tables 3 and 4, have been tabulated. The large discrepancy noted above in the point by point comparisons cannot be explained by these parametric differences however, since they would increase the new theoretical values of  $Q_1$  by no more than 3 or 4 percent.

Although it is possible that the discrepancies found between these results and the Monte Carlo calculations are due to some undetected systematic error, we feel it is more likely that they are due to the use of the Klein-Nishina cross sections. Considering only the incoherent scattering from free electrons is an oversimplification which is not physically accurate. While most of the neglected processes contribute only a small amount to penetration data it is expected<sup>6</sup> that these effects might show up in comparisons between theoretical and experimental albedo values.

---

\* Private communication.

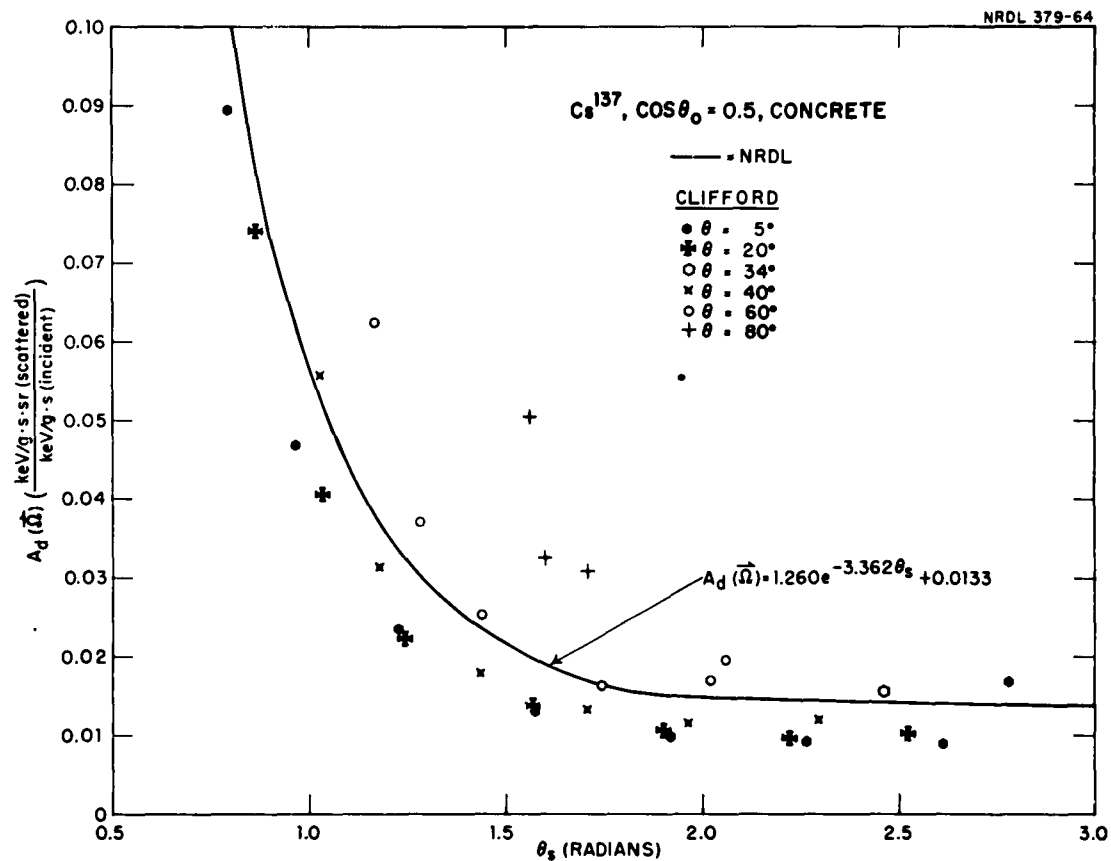


Fig. 11 Comparison of Clifford with NRDL;  $A_d(\vec{\Omega})$  vs.  $\theta_s$ . The experimental data of Clifford<sup>6</sup> are plotted with symbols corresponding to the  $\theta$  angles at which they were taken.

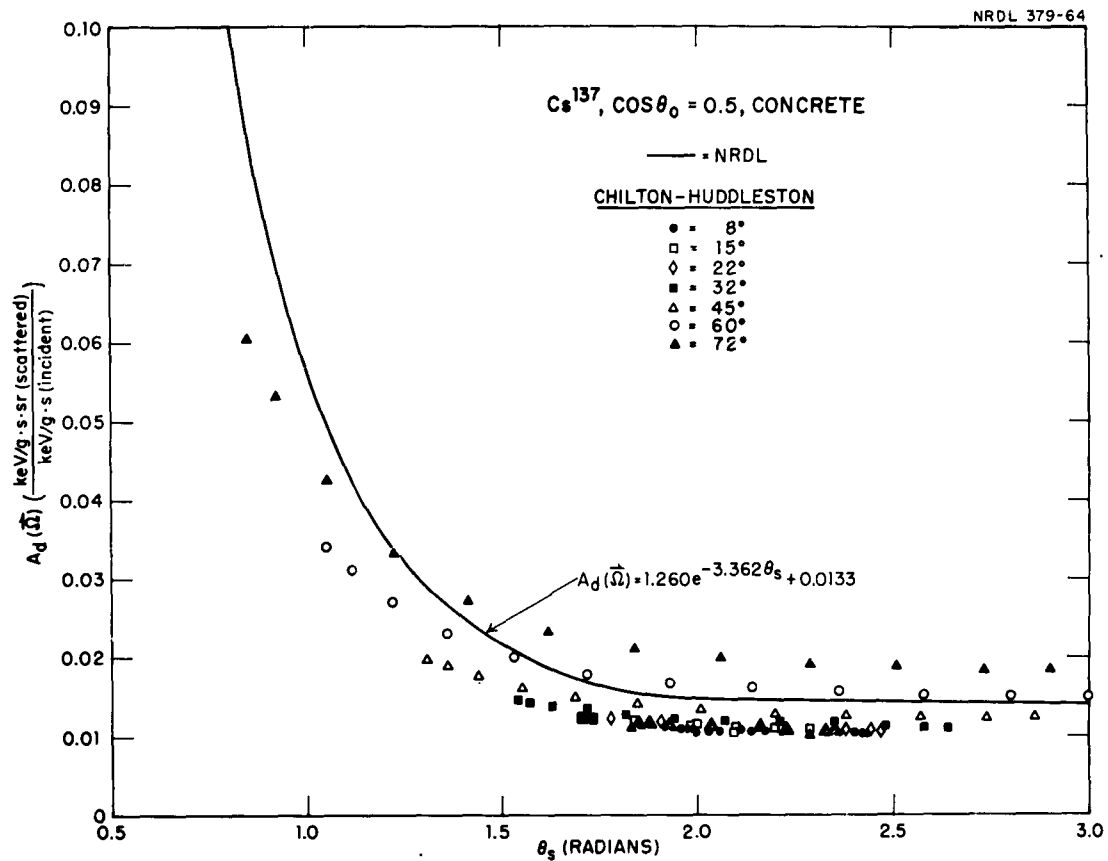


Fig. 12 Comparison of Chilton-Huddleston with NRDL;  $A_d(\vec{\Omega})$  vs.  $\theta_s$ . The calculated data of Chilton-Huddleston are plotted with symbols corresponding to the  $\theta$  angles for which they were calculated.

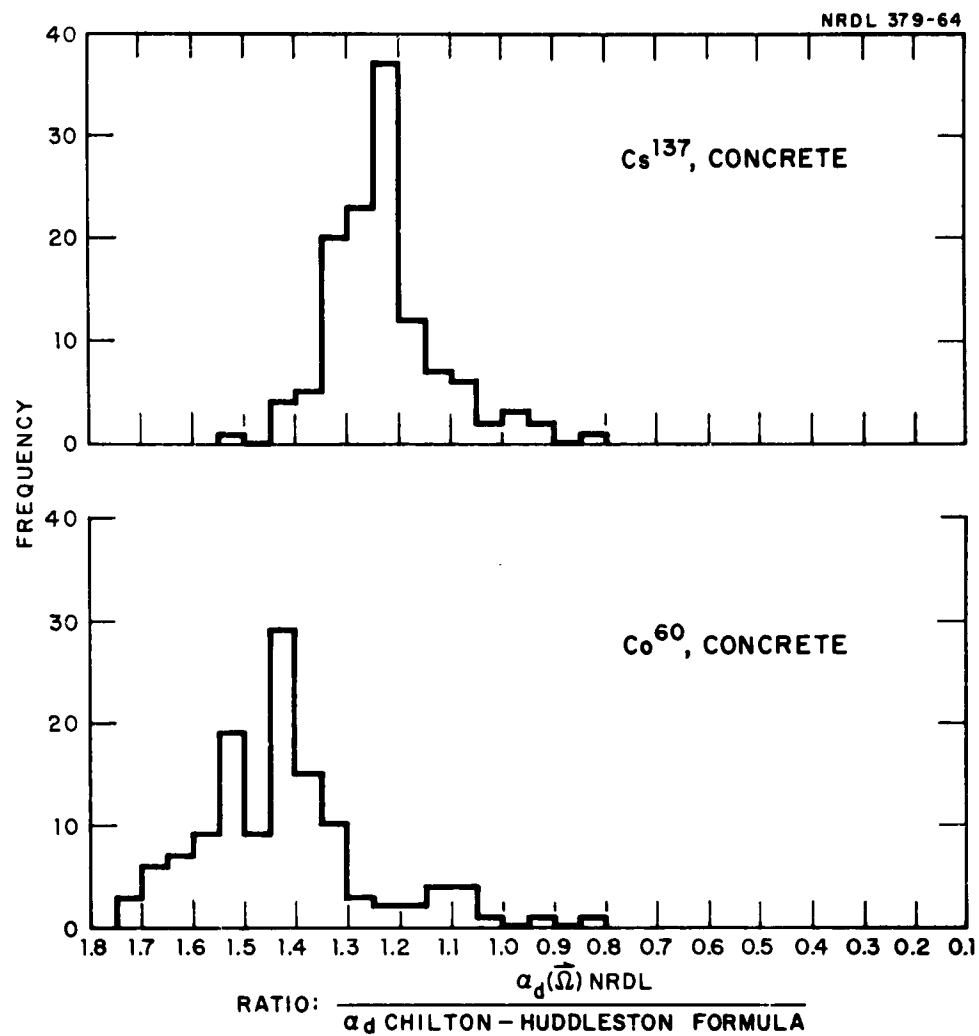


Fig. 13 Histograms of the Comparison Ratio Distributions,  
 $\frac{\alpha_d(\vec{n}) \text{ (NRDL)}}{\alpha_d \text{ (Chilton-Huddleston formula)}}$

## APPENDIX I

### DISCUSSION OF ALBEDO

#### A. General

Literally, albedo means whiteness; technically, it is a reflection coefficient. It has been appropriated from its original usage in astronomy and optics to help describe gamma-ray scattering. Since, in contrast to light photons, gamma photons interact throughout a volume rather than at a surface, the concept of gamma albedo needs to be examined closely.

#### B. Notation

We follow the notations of Goldstein<sup>8</sup> and Raso<sup>4</sup> where possible. The current-reflection coefficient (albedo) is always represented by the symbol  $\alpha$ , the flux-reflection coefficient by A, flux density by I and current density by J. The subscripts n and d denote number and dose, respectively. These and other symbols used in this report are listed alphabetically in the glossary.

Degrees of differentiation of a functional quantity will be represented by the number of variables appearing as arguments of the function. Thus:  $\alpha_n(\vec{r}, \vec{\Omega}, h\nu)$  is differential angular energy dose albedo.

#### C. Definitions

The fundamental physical quantity in gamma-ray transport is the flow of photons. Specifically:

$$\text{I-1} \quad I_n(\vec{r}, \vec{\Omega}, h\nu) \quad \left[ \text{photons} \cdot \text{cm}^{-2} \cdot \text{s}^{-1} \cdot \text{ster}^{-1} \cdot \text{kev}^{-1} \right]$$

is the differential angular energy distribution of the photon number

flux density and, when multiplied by  $d\Omega(h\nu)$ , will give the number of photons/s crossing a unit area at  $\vec{r}$  whose normal lies along the unit direction vector  $\vec{n}$ , the photons' energies lying between  $h\nu$  and  $h\nu+d(h\nu)$  and their directions along  $\vec{n}$  within the solid angle  $d\Omega$ . See Fig. 14. For the description of albedos or reflection coefficients it is convenient to set up the coordinate axes so that the reflecting surface is the xy plane and so that the point of intersection of the source collimator axis with this plane determines the origin.

For this experiment the experimental quantities are independent of x and y and  $z \equiv 0$  since we have placed the origin of our coordinate system at the surface. We thus drop  $\vec{r}$  and write  $I_n(\vec{n}, h\nu)$ .

If the reference unit area at the origin remains in the back-scattering surface as  $\vec{n}$  varies, we have a different quantity called angular energy number current density, which is related to angular energy flux density by:

$$I-2 \quad J_n(\vec{n}, h\nu) = I_n(\vec{n}, h\nu) \cos\theta$$

where  $\theta$  is the angle between  $\vec{n}$  and the surface normal.

#### D. Integral Albedo

If, in a time  $t$ ,  $N^{(o)}$  incident gamma photons penetrate a surface area,  $a$ , of a medium; and if, after scattering in the medium,  $N$  photons come back out through the same area; then, the integral gamma-ray number albedo for these incident photons and this medium is defined to be:

$$I-3 \quad \alpha_n \equiv N/N^{(o)}.$$

Note that in this example the incident current density,  $J_n^{(o)} = N^{(o)} a^{-1} t^{-1}$  and the reflected current density is just  $J_n = N a^{-1} t^{-1}$ . Thus we see that albedo may be defined as a ratio of current densities since:

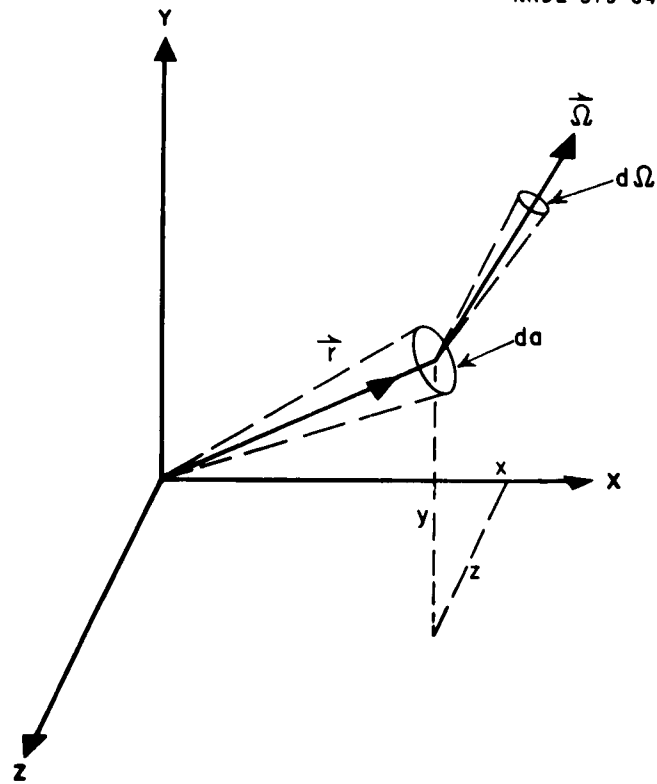


Fig. 14 Space Diagram.



$$I-4 \quad \frac{J_n}{J_n(o)} = \frac{N/at}{N(o)/at} = \frac{N}{N(o)} = \alpha_n.$$

#### E. Differential Albedo

One could define many differential albedos, each one corresponding to different combinations of incident and scattered currents of number, energy or dose, each being partially or totally differentiated with respect to direction and energy. Of these many possibilities the albedo quantity reported in this experiment is the angular dose albedo for an "infinitely" thick\* slab irradiated by an "infinitely" broad\*\* beam of approximately parallel gamma rays. Symbolically:

$$I-5 \quad \alpha_d(\vec{n}) = \frac{\int_0^{\infty} J_d(\theta, \phi, hv) d(hv)}{\int_0^{\pi} \int_0^{2\pi} \int_0^{\infty} J_d^{(o)}(\theta', \phi', hv') \sin \theta' d\theta' d\phi' d(hv)}$$

where:

$$J_d(\theta, \phi, hv) = I_d(\theta, \phi, hv) \cos \theta; \quad I_d(\theta, \phi, hv)^{***} = hv \cdot \frac{\mu_a(hv)}{\rho} \cdot I_n(\theta, \phi, hv).$$

$\left(\frac{\mu_a(hv)}{\rho}\right)$  is the air energy mass-absorption coefficient.)

\* No effect is observed when additional slab material is added.

\*\* No effect is observed when the beam radius is increased.

\*\*\*  $I_d(\vec{n}) = \int_0^{\infty} I_d(\theta, \phi, hv) d(hv)$  is the differential angular first collision air absorbed "dose" rate; referred to as angular dose rate.

Since, in this experiment, the source gamma rays were both mono-directional and monoenergetic,

$$J_d^{(o)}(\theta', \phi', h\nu') = (J_d)_o \delta(\theta' - \theta_o) \delta(\phi') \delta(h\nu' - h\nu_o)$$

where

$$(J_d)_o \equiv J_d^{(o)}(\theta_o, 0, h\nu_o).$$

Integration of I-5 then yields

$$\text{I-6} \quad \alpha_d(\vec{\Omega}) = \frac{J_d(\vec{\Omega})}{(J_d)_o}.$$

This differential albedo is identical to Rasos's<sup>4</sup>  $\alpha_d$ .

## APPENDIX II

### EXPERIMENTAL APPARATUS AND METHODS

#### A. Experimental Design

The quantity to be determined,  $\alpha_q(\Omega)$ , imposes several conditions upon the experimental apparatus and method. First, the solid angle (at the center of the slab face) subtended by the dosimeter should be small since the experimental results are to be differential in scattering angle. Second, the slab area "seen" by the dosimeter should be well defined since this area is used to convert dose rate to "dose-current." Third, the slab area and thickness should be "infinitely" large, as noted in Appendix I. Fourth, the slab should be uniformly irradiated. The experimental configuration chosen to satisfy these conditions is shown in Fig. 15a.

Specifically, the first condition was met by using a lead-shielded plastic scintillation detector with a collimator in the form of a long cylindrical hole in the detector shield. The solid angle subtended at the center of the slab face by the exposed area of the scintillator has been determined to be 223  $\mu$ -steradians (see Fig. 15b). Because of the small cross section for backscattering, the extremely small solid angle subtended by the detector and available source-strengths ( $\text{Co}^{60}$ ,  $\sim 11.5$  curies;  $\text{Cs}^{137}$ ,  $\sim 8$  curies), the level of dose rate measured in this experiment was from 0.2 to 2.0 mr/hr. To accomplish this measurement with some degree of reliability in a reasonable length of time it was necessary to use a scintillation dosimetry system similar to that used by Dahlstrom.<sup>3</sup>

Although the second condition could be met by increasing the (collimator length)/(detector distance) ratio, the resulting detector-shield weight and interference with the incident beam make this solution impractical. The relationships between the irradiated area of the slab and the effective "viewed" area are shown in Fig. 15c and are discussed in detail in reference 3.

While the umbral area is only  $0.44 \text{ sec}\theta \text{ in}^2$  the penumbral region increases the effective "viewed" area ( $a \text{ sec}\theta$ ) to  $10.78 \text{ sec}\theta \text{ in}^2$  and thus the detection solid angle ( $\Omega_\epsilon = a_\epsilon/R^2$ ) to 5330  $\mu$ -steradians.

## APPENDIX II

### EXPERIMENTAL APPARATUS AND METHODS

#### A. Experimental Design

The quantity to be determined,  $\alpha_q(\Omega)$ , imposes several conditions upon the experimental apparatus and method. First, the solid angle (at the center of the slab face) subtended by the dosimeter should be small since the experimental results are to be differential in scattering angle. Second, the slab area "seen" by the dosimeter should be well defined since this area is used to convert dose rate to "dose-current." Third, the slab area and thickness should be "infinitely" large, as noted in Appendix I. Fourth, the slab should be uniformly irradiated. The experimental configuration chosen to satisfy these conditions is shown in Fig. 15a.

Specifically, the first condition was met by using a lead-shielded plastic scintillation detector with a collimator in the form of a long cylindrical hole in the detector shield. The solid angle subtended at the center of the slab face by the exposed area of the scintillator has been determined to be 223  $\mu$ -steradians (see Fig. 15b). Because of the small cross section for backscattering, the extremely small solid angle subtended by the detector and available source-strengths ( $\text{Co}^{60}$ ,  $\sim 11.5$  curies;  $\text{Cs}^{137}$ ,  $\sim 8$  curies), the level of dose rate measured in this experiment was from 0.2 to 2.0 mr/hr. To accomplish this measurement with some degree of reliability in a reasonable length of time it was necessary to use a scintillation dosimetry system similar to that used by Dahlstrom.<sup>3</sup>

Although the second condition could be met by increasing the (collimator length)/(detector distance) ratio, the resulting detector-shield weight and interference with the incident beam make this solution impractical. The relationships between the irradiated area of the slab and the effective "viewed" area are shown in Fig. 15c and are discussed in detail in reference 3.

While the umbral area is only  $0.44 \text{ sec}\theta \text{ in}^2$  the penumbral region increases the effective "viewed" area ( $a \text{ sec}\theta$ ) to  $10.78 \text{ sec}\theta \text{ in}^2$  and thus the detection solid angle ( $\Omega_e = a_e/R^2$ ) to 5330  $\mu$ -steradians.



Fig. 15a Experimental Configuration. The  $\text{Cs}^{137}$  source is positioned for an incidence angle of  $\arccos 0.50$ . The detector is positioned for  $\theta = 45^\circ$  and  $\phi = 112.5^\circ$ . The slab material is concrete. The  $\text{Co}^{60}$  source is shown stored and secured.

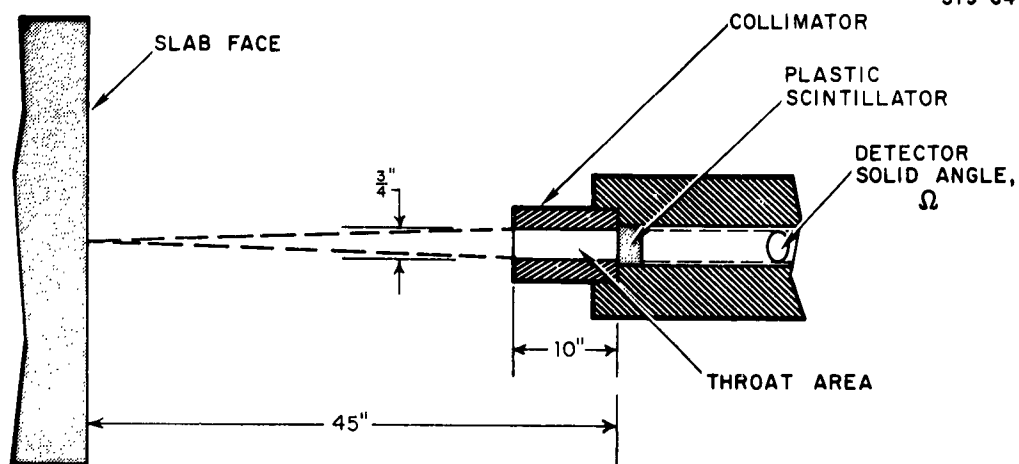


Fig. 15b Slab-Detector Geometry.

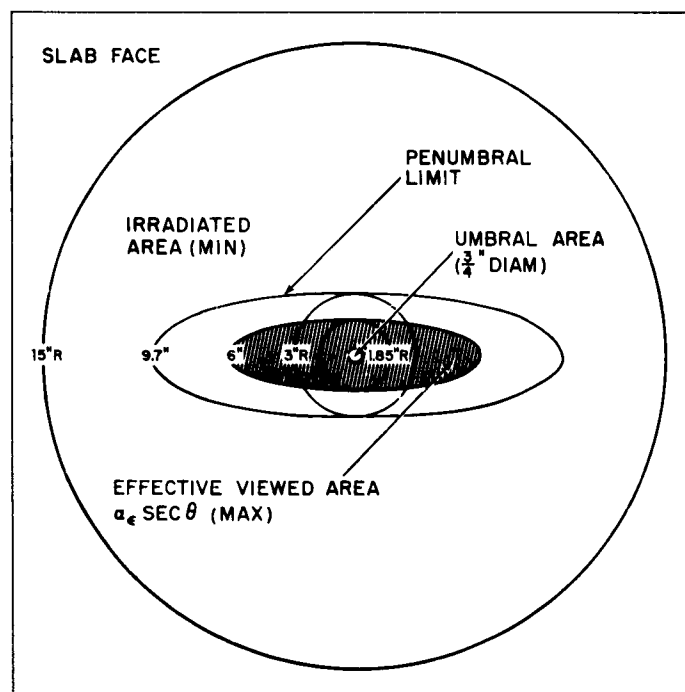


Fig. 15c Irradiated and "Viewed" Areas of the Slab.

The third condition, implied by specifying the slab geometry as semi-infinite, means that any increase in the irradiated slab area or the slab thickness must not result in a change in the albedo from the viewed area. A minimum irradiated circular area of 15 in. radius and slab thicknesses of 4 mean free paths or greater, coupled with a maximum "viewed" area having a semi-major axis of 6 in. were chosen to satisfy this condition.<sup>9</sup>

By "uniformly irradiated" in condition four we mean that the incident gamma rays are essentially monoenergetic, monodirectional and of equal flux density over the irradiated area. Condition four was approximately satisfied by placing collimated Cs<sup>137</sup> and Co<sup>60</sup> "point" isotropic sources at a distance of 97 in. from the slab.<sup>6</sup> The dose rates, measured by calibrated Landsverk and Baldwin-Farmer dosimeters, under these conditions were  $5.25 \times 10^6$  and  $2.11 \times 10^7$  keV/gm sec for Cs<sup>137</sup> and Co<sup>60</sup> respectively. These quantities, adjusted for decay during the course of the experiment, are the incident dose rates,  $(I_d)_0$ , used in calculating  $\alpha_d(\bar{\Omega})$ .

## B. Dosimetry System

The essential details concerning the detection system used in this experiment, the calibration of the system, and the means by which the output of the system is converted into detected dose rate is reported here. First, the sections shown in Fig. 16 are discussed, followed by preoperation calibration, dosimetry system calibration, and data acquisition and recording.

### 1. Detector.

The gamma sensor is a 1 in. diameter by a 1 in. height plastic scintillator of a polymerized solution of p-terphenyl and tetraphenylbutadiene in styrene.

The thickness of the lead shielding around the plastic scintillator varied from 10 in. in the forward direction to 3 in. at the sides. A 3/4 in. diameter by 10 in. long aperture in the shielding acted as a collimator to define both the exposed frontal area of the scintillator and the "viewing" solid angle of the detector.

The light from this scintillator is converted into current pulses by a 14-stage EMI-9536S photomultiplier operated at 1100 volts. The photomultiplier output is coupled to a two-stage Franklin pre-amplifier. The first stage, a one tube class A amplifier, is DC coupled to a cathode follower. The overall preamplifier gain is 3 with

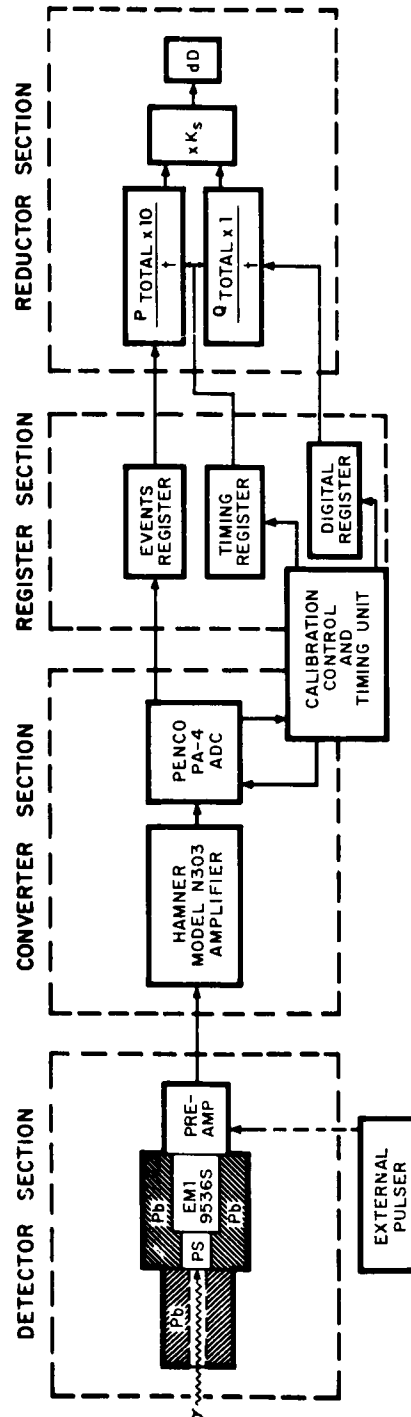


Fig. 16 Dosimetry System Diagram.



sufficient negative feedback to provide excellent gain stability.

The output impedance of the preamplifier is low to match the impedance of the 25 ft length of coaxial cable connecting the detector and the converter sections.

## 2. Converter.

The converter section is composed of a Hamner Model N 303 non-overloading, linear amplifier, the analog to digital converter unit (ADC) from a Penco Model PA-4 pulse-height analyzer and a NRDL Model 1 Calibration and Control Unit. An upper bound discriminator was added to the ADC to reject pulses exceeding the upper bound voltage,  $V_u$ .

The amplifier gain was standardized to spread the pulse-height distribution from 350 keV photons over the full 100 volt ADC range. (See Fig. 17.)

With this standard system amplification some pulses exceed the upper bound voltage for photon energies above 350 keV. By adjusting the amplifier gain to one half its standard value and raising the lower ADC discriminator level to  $1/2 V_u$  it is possible to convert only these excess pulses for photon energies up to 700 keV. By this two gain technique the dosimetry system is able to handle the range of photon energies of interest in this experiment.

The ADC unit will convert any analog pulse greater than the minimum threshold,  $V_T = 4$  volts and less than the upper bound voltage,  $V_u = 104.5$  volts. For each conversion process an events pulse is generated. In the amplitude to time conversion process a one megacycle/s pulse generator is gated on for a length of time related to the peak voltage amplitude,  $V$ , attained by the analog pulse. The relationship is such that the number of digital pulses,  $q$ , in this pulse train is numerically equal to the quantity  $(\bar{V} - \bar{V}_T)$  where the bar indicates that  $V - V_T$  is rounded off to the nearest integer voltage.

Thus, the presence of the threshold produces aberrations in the response in two ways: No pulse less than 4 volts in height is converted; and each  $q$  is 4 units smaller than the corresponding analog pulse height. Corrections for these threshold effects have been incorporated into the dose-rate formula of the reductor and are discussed in Section D (Dosimetry System Calibration).

## 3. Register.

The digital register accumulates the digital pulses,  $q$ , generated by the converter. The total number of such pulses accumulated

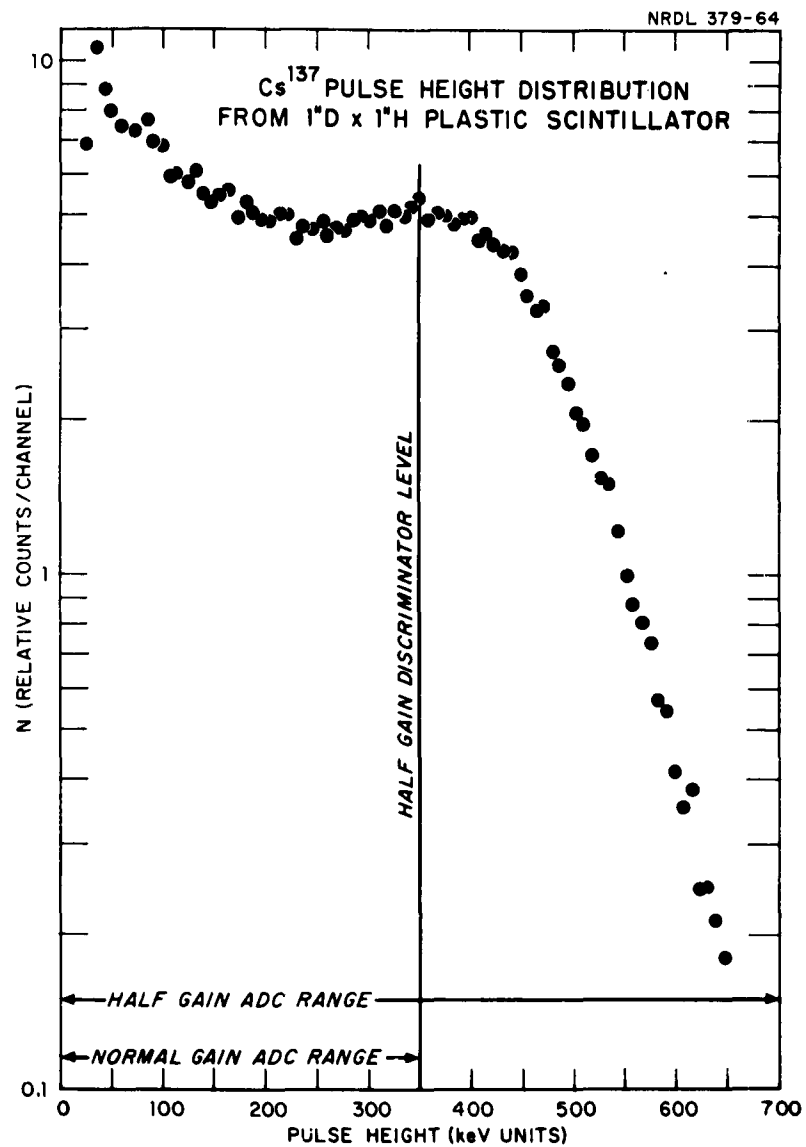


Fig. 17 Pulse-Height Distribution. The distribution is of the response of the 1 in. diameter by 1 in. height plastic scintillator, used in the experiment, to  $\text{Cs}^{137}$  gamma rays.

in a time  $t$  is designated by  $Q = \Sigma q$ .

The events register accumulates the events,  $P$ , converted in time  $t$ .

The timing register accumulates the total number of kc/s pulses generated by the live-timing circuit. Thus, the timing register divided by a thousand gives the elapsed counting time,  $t$ , in seconds.

#### 4. Reductor.

In the reductor the registered quantities  $Q$ ,  $P$  and  $t$  are combined to give detected dose rate by the formula:

$$dD = K_s \left( \frac{Q_{\text{total}}}{t} + T \frac{P_{\text{total}}}{t} \right) \left[ \text{keV} \cdot \text{g}^{-1} \cdot \text{s}^{-1} \right]$$

$$Q_{\text{total}} = Q_s + 2Q_{s/2} \text{ and } P_{\text{total}} = P_s + 2P_{s/2}$$

where:  $Q_s$  and  $P_s$  are, respectively, the net registered digital pulses and the net registered events for the standard mode; and  $Q_{s/2}$  and  $P_{s/2}$  are, respectively, the net registered digital pulses and the net registered events above the standard mode upper bound taken with half-standard gain.  $K_s$  is an empirically determined dose-rate conversion factor and  $T$  is a threshold correction parameter.

It should be noted that the values of  $K_s$  and  $T$  are of critical importance in this experiment since they convert the system into a dosimeter. The determination of these values will therefore be discussed at some length. However, prior to this discussion, it is desirable to dispense with the details associated with the preoperation calibration of the electronics.

In addition to the above sections a calibration, control and timing unit serves to make the dosimetry system operable. It provides a method for calibrating the system, a preset live-time capability and certain control functions not found in the PA-4 ADC unit.

### C. Preoperation Calibration

#### 1. ADC Calibration.

Reference voltage, channel linearity, channel width and threshold checks of the ADC unit were made as specified in the Penco PA-4 Instruction Manual.

The upper bounds circuit of the ADC was adjusted to prevent the conversion of any analog pulse which would give a digital pulse train value,  $q$ , greater than 100. Since the range of analog pulse voltage amplitudes which are converted to a  $q$  of 100 is from 103.5 v to 104.5 v, this adjustment was performed while converting 104.5 v pulses from external 60 c/s pulse generator. Because there is a symmetrical distribution of pulses around the average value of 104.5 v, half of these pulses should be converted if the upper bound discriminator is working properly. Thus an events scaler rate  $p/t$  of  $30 \text{ s}^{-1}$  was the objective in adjusting the upper bound discriminator.

## 2. Linearity and Threshold.

Upon completion of the ADC calibration, an investigation of the linearity and threshold of the system from the preamplifier through the ADC was made. Ten second sampling periods were used to measure  $Q$  and  $P$  values for various pulser settings. A plot of  $\bar{q} = Q/P$  versus pulser setting resulted in a linearity curve with the threshold being the intercept. Figure 18 is a plot of typical results.

### D. Dosimetry System Calibration

Ideally, the accumulated digital counts,  $Q_{\text{total}}$ , divided by the counting time  $t$  is proportional to  $dD$ .<sup>10</sup> However, as mentioned in the converter discussion, the threshold of the ADC unit introduces two types of aberration. The threshold subtractive effect reduces each analog pulse voltage by 4 volts and the threshold loss effect ignores a fraction of the input pulses. This fraction increases as the photon energy,  $h\nu$ , decreases. In addition, the fraction of energy absorbed in the plastic scintillator due to multiple collisions, rather than first collisions, also increases as the photon energy,  $h\nu$ , decreases. The formula,

$$dD = K_B \left( \frac{Q_{\text{total}}}{t} + T \frac{P_{\text{total}}}{t} \right),$$

of the reductor section is an attempt to compensate for these energy dependent aberrations. The method of determining  $K_B$  by adjusting  $T$ , to minimize these aberrations, follows.

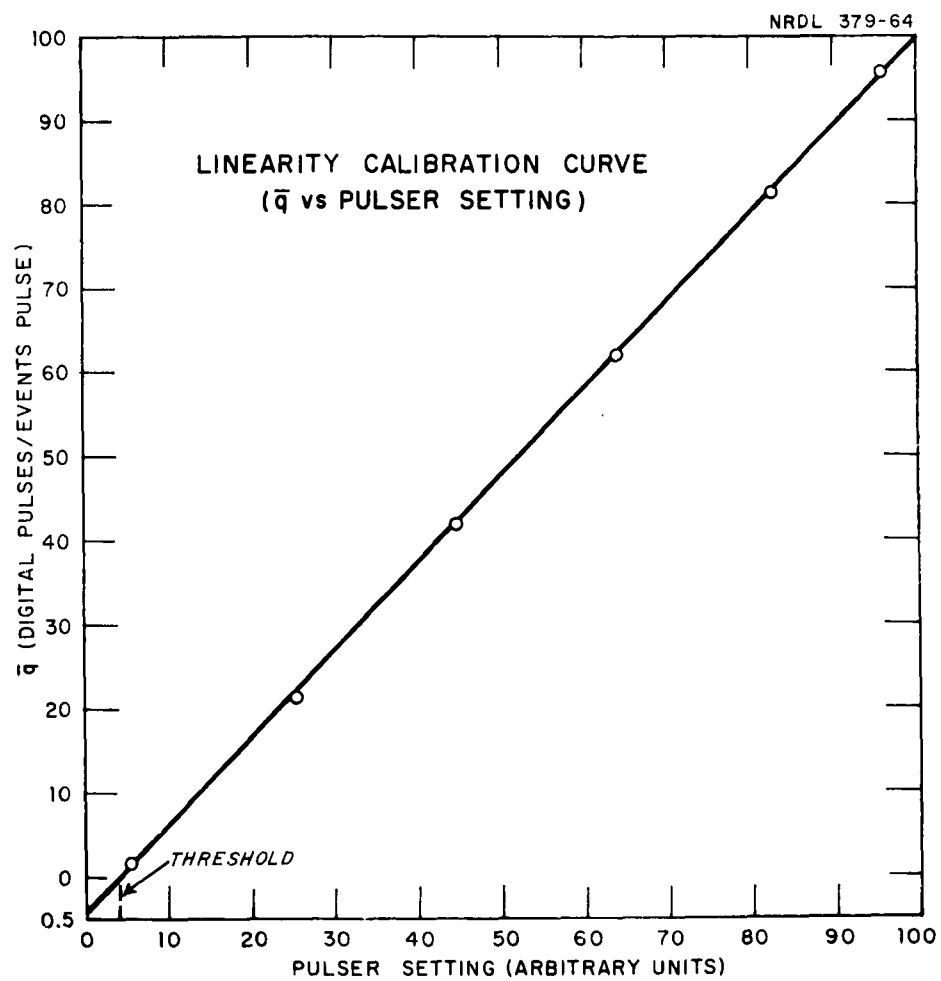


Fig. 18 Linearity Calibration Curve.

Four calibration sources were used, each producing monoenergetic gamma rays. Each source was placed on the collimator axis as shown in Fig. 19. The dosimeter measurements

$$\left( \frac{Q_{\text{total}}}{t} \right)_i \text{ and } \left( \frac{P_{\text{total}}}{t} \right)_i$$

were taken for each calibration gamma photon energy,  $h\nu_i$ .

Without disturbing the source and detector shield geometry the plastic scintillator and photomultiplier were replaced by a 1 in. by 1 in. diameter NaI(Tl) scintillator and photomultiplier. The amplified output pulses from this detector were analyzed and recorded by a Penco PA-3 analyzer. From these pulse-height distributions and the known detection efficiency and detection area of the NaI detector, the incident photon-number-flux density,  $I_n(h\nu)_i$ , was calculated for each source. The dose rate at the detector was calculated by the formula:

$$I_d(h\nu)_i = \left[ h\nu \frac{\mu_a}{\rho}(h\nu) I_n(h\nu) \right]_i.$$

Dose-rate conversion factors for each calibration gamma photon energy,  $h\nu_i$ , were calculated by the formula:

$$K(h\nu, T)_i = \left[ I_d(h\nu) / \left( \frac{Q_{\text{total}}}{t} + T \frac{P_{\text{total}}}{t} \right) \right]_i$$

for several values of T.

Figure 20 shows the energy dependence of  $K(h\nu, T)$  for four values of T.  $T = 10$  was the final value chosen to calculate each  $K(h\nu)_i$ . The system dose-rate conversion factor,  $K_s$ , was obtained by taking a simple average of the four  $K(h\nu, 10)_i$  factors:

$$K_s = 1/4 \sum_{i=1}^4 K(h\nu, 10)_i = 0.440 \pm 0.006.$$

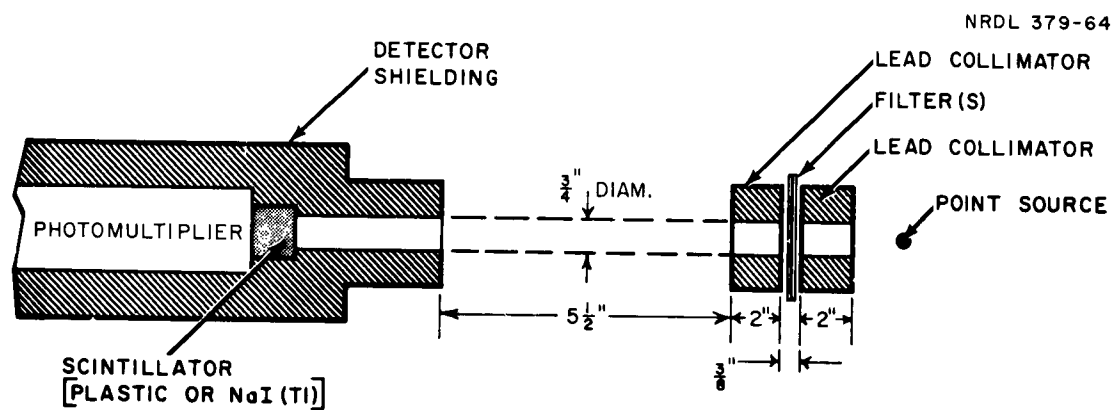


Fig. 19 Dosimetry System Calibration Geometry.

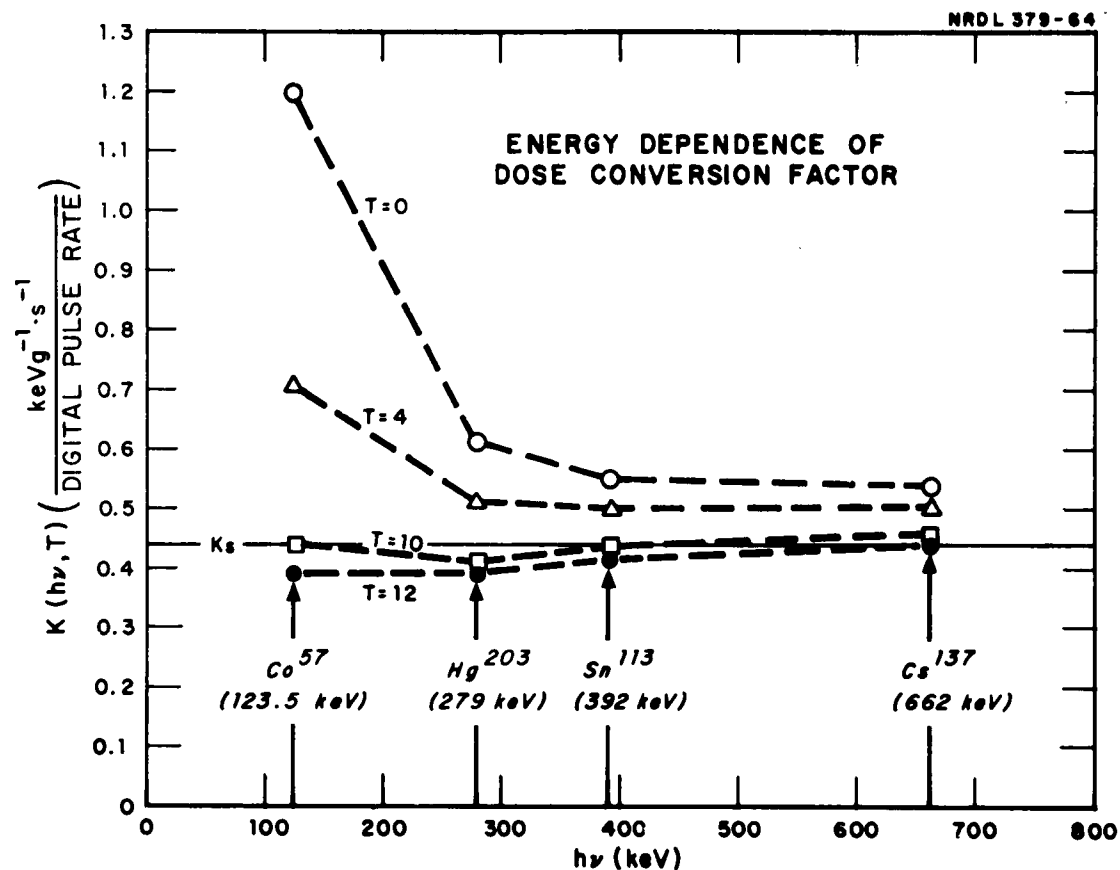


Fig. 20 Energy Dependence of Dose Conversion Factor. The set of points marked  $T = 0$  shows the uncorrected factor. The points labeled  $T = 4$  are corrected for the threshold subtractive aberration. The points for  $T = 10$ , the value finally adopted compensates for the threshold loss aberration. The points for  $T = 12$  shows the effect of an additional compensation. The solid line labeled  $K_s$  is an average of the four  $T = 10$  points and is the system dose conversion factor used in formula of the reductor section.



Inserting these values of  $K_s$  and  $T$  into the formula of the reductor section we have:

$$dD = 0.440 \left( \frac{Q_{\text{total}}}{t} + 10 \frac{P_{\text{total}}}{t} \right) \left[ \text{keV gm}^{-1} \text{ s}^{-1} \right].$$

#### E. Data Acquisition and Recording

The variable parameters were the radiation sources,  $\text{Cs}^{137}$  and  $\text{Co}^{60}$ ; the slab materials, concrete, aluminum and steel; the incidence angles,  $\theta_o = \cos^{-1} 1.00, 0.75, 0.50$ ; and the detection angles,  $\theta = 8^\circ, 15^\circ, 22^\circ, 32^\circ, 45^\circ, 60^\circ$  and  $72^\circ$  and  $\phi = 7.5^\circ, 22.5^\circ, 37.5^\circ, 52.5^\circ, 67.5^\circ, 82.5^\circ, 97.5^\circ, 112.5^\circ, 127.5^\circ, 142.5^\circ, 157.5^\circ$  and  $172.5^\circ$ .

An almost complete set of data for all detection angles was taken for the concrete, but for the aluminum and steel, measurements were taken for selected values of  $\theta$  and  $\phi$ .

The slabs were exposed and data were taken for sampling times of 1000 seconds. For each combination of the variable parameters described above a foreground and background was made at standard gain and, where necessary, at half standard gain. The background runs were made with the source "on" but with a lead plug in the detector collimator.

The net readings ( $Q_{\text{foreground}} - Q_{\text{background}}$ ) and ( $P_{\text{foreground}} - P_{\text{background}}$ ) were combined to give the dose rate at the detector.

Daily checks were made of the system amplification by feeding calibration pulses of a standard amplitude into the preamplifier in the same way as for the linearity and threshold calibration. Any shift noted was compensated for by adjusting the amplifier fine gain control. Following this adjustment, the overall system gain was measured by making a  $\bar{q}$  measurement for a  $\text{Hg}^{203}$  calibration source. The distribution of the daily  $\text{Hg}^{203}$   $\bar{q}$  values had a maximum variation from the average of less than 1 percent during the period of data taking.

## REFERENCES

1. Scofield, N. E. and Haggmark, L. G., "Penetration of Plane Normal and Plane Slant Gamma Rays Through Slabs of Aluminum and Steel. II. Angular and Energy Spectra (Photon Number Flux)." USNRDL-TR-475 (October 1960).
2. Lynn, R. L. and Scofield, N. E., "Gamma-Ray Slab Penetration Dose Build-Up Factor Measurements (U)." SECRET-RESTRICTED DATA, ANP Document NARF-59-14T, FZK-9-137, Vol. I (1959).
3. Dahlstrom, T. S. and Thompson, W. E., "The Angular Distributions of Dose Rate from Gamma Rays Scattered Through Various Thicknesses of Iron and Aluminum." USNRDL-TR-558 (April 1962).
4. Raso, D. J., "Monte Carlo Calculations on the Reflection and Transmission of Scattered Gamma Rays." Nuc. Sci. Eng. 17, 411 (1963).
5. Chilton, A. B. and Huddleston, C. M., "A Semiempirical Formula for Differential Dose Albedo for Gamma Rays on Concrete." Nuc. Sci. Eng. 17, 419 (1963).
6. Clifford, C. E., "Differential Dose Albedo Measurements for 0.66 MeV  $\gamma$ 's Incident on Concrete, Iron and Lead (U)." Defence Research Chemical Laboratories Report 412, Ottawa, Canada (August 1963).
7. Spencer, L. V., Proceedings and Final Report, Summer Institute on Fundamental Radiation Shielding Problems, Department of Nuclear Engineering, Kansas State University, Manhattan, Kan. (1962).
8. Goldstein, H. and Wilkins, J. E., Jr., "Calculations of the Penetration of Gamma Rays." NYO-3075, Nuclear Defense Associates, Inc., White Plains, N. Y., 30 June 1954.
9. Scofield, N. E., Lynn, R. L., and Kreger, W. E., "Penetration of Plane Normal and Plane Slant Gamma Rays Through Slabs of Aluminum and Steel. I. Angular and Energy Distributions (Experimental Pulse Height)." USNRDL-272 (October 1958).
10. Whyte, G. N., Principles of Radiation Dosimetry, New York, N. Y., John Wiley and Sons, Inc., 1959, pp. 109ff.

## Physics and Shielding

### INITIAL DISTRIBUTION

#### Copies

##### NAVY

1	Chief, Bureau of Ships (Codes 320-364A)
2	Chief, Bureau of Ships (Code 210L)
1	Chief, Bureau of Ships (Code 423)
1	Chief of Naval Operations (Op-07T10)
1	CO-Dir., Naval Applied Science Lab. (Code 962)
3	Dir., Naval Research Laboratory
1	CO-Dir., Naval Civil Engineering Laboratory
1	CO, Naval Civil Engineering Corps Officers School
3	CO, Office of Naval Research, FPO, New York
1	Supt., Naval Postgraduate School, Monterey

##### ARMY

1	Chief of Research and Development (Atomic Office)
2	Commander, Nuclear Defense Laboratory (Lib., Donnert)
1	CO, Army Electronic Res. and Dev. Laboratory
2	CG, Ballistic Research Laboratory (Allen, Ethridge)
4	Office of Civil Defense (Buchanan, FitzSimmons, Stangler, Greene)

##### AIR FORCE

1	Chief, Systems Engineering Group (SEPIR)
1	Dir., USAF Project RAND
1	Dir., Air University Library, Maxwell AFB
1	Commander, AF Cambridge Research Labs. (CRT)

##### OTHER DOD ACTIVITIES

3	Dir., Defense Atomic Support Agency (Lib., Daniel)
1	Commander, FC/DASA, Sandia Base (FCTG5, Lib.)
20	Defense Documentation Center

##### AEC ACTIVITIES AND OTHERS

4	Argonne National Laboratory (Library, Grotenhuis)
3	Atomic Energy Commission, Washington

1       Atomics International (Ashley)  
 2       Battelle Memorial Institute  
 4       Brookhaven National Laboratory  
 2       Los Alamos Scientific Lab. (Library)  
 1       National Aeronautical Space Administration (Reetz)  
 1       NASA, Lewis Research Center  
 1       National Academy of Sciences (Park)  
 3       National Bureau of Standards (Library, Eisenhower, Berger)  
 1       New York University (Kalos)  
 5       Oak Ridge National Laboratory (Auxier, Zobel, Clifford, Blizzard, Penny)  
 2       Radiation Research Associates (Wells, Schaeffer)  
 1       Sandia Corporation, Albuquerque  
 1       Sandia Corporation, Livermore  
 2       Technical Operations, Inc. (Clarke, Tiller)  
 1       University of Illinois (Chilton)  
 2       U. of California Lawrence Radiation Lab., Livermore  
 2       U. of California Lawrence Radiation Lab., Berkeley  
 1       United Nuclear Corporation (Mittleman)  
 25      Division of Technical Extension, Oak Ridge

USNRDL

40       Technical Information Division

DISTRIBUTION DATE: DEC 15 1964

<p>Naval Radiological Defense Laboratory USNRDL-TR-790</p> <p>EXPERIMENTAL DETERMINATION OF THE GAMMA-RAY ANGULAR DOSE ALBEDOS OF CONCRETE, ALUMINUM AND STEEL, by T. H. Jones, N. E. Scofield, L. G. Haggmark, and W. J. Gurney 6 October 1964 63 p. illus. tables 10 refs. UNCLASSIFIED</p> <p>The angular distribution of dose albedo was measured for "semi-infinite" concrete, aluminum and steel slabs irradiated by plane-parallel beams of Co<sup>60</sup> and Cs<sup>137</sup> gamma photons. The photons were incident on the slabs at angles, measured from a normal to the slab, of arccos 1.00, 0.75 and 0.50. For the necessary sensitivity, the reflected dose rate was (over)</p>	<p>1. Gamma-ray scattering. 2. Steel - Bombardment. 3. Aluminum - Bombardment. 4. Concrete - Bombardment. 5. Reactor shielding materials. I. Jones, T. H. II. Scofield, N. E. III. Haggmark, L. G. IV. Gurney, W. J. V. Title. VI. SF 011 05 11.</p> <p>UNCLASSIFIED</p>
<p>measured by a digital dosimetry system using a plastic scintillator as the detector.</p> <p>An empirical formula for angular dose albedo was derived from the experimental data. Comparisons are made with the Monte Carlo calculations of D. J. Raso and the experimental results of C. E. Clifford (DRCL).</p> <p>UNCLASSIFIED</p>	<p>measured by a digital dosimetry system using a plastic scintillator as the detector.</p> <p>An empirical formula for angular dose albedo was derived from the experimental data. Comparisons are made with the Monte Carlo calculations of D. J. Raso and the experimental results of C. E. Clifford (DRCL).</p> <p>UNCLASSIFIED</p>

<p>Naval Radiological Defense Laboratory USNRDL-TR-790</p> <p>EXPERIMENTAL DETERMINATION OF THE GAMMA-RAY ANGULAR DOSE ALBEDOS OF CONCRETE, ALUMINUM AND STEEL, by T. H. Jones, N. E. Scofield, L. G. Haggmark, and W. J. Gurney 6 October 1964 63 p. illus. tables 10 refs. UNCLASSIFIED</p> <p>The angular distribution of dose albedo was measured for "semi-infinite" concrete, aluminum and steel slabs irradiated by plane-parallel beams of Co<sup>60</sup> and Cs<sup>137</sup> gamma photons. The photons were incident on the slabs at angles, measured from a normal to the slab, of arccos 1.00, 0.75 and 0.50. For the necessary sensitivity, the reflected dose rate was</p> <p>(over)</p> <p>1. Gamma-ray scattering. 2. Steel - Bombardment. 3. Aluminum - Bombardment. 4. Concrete - Bombardment. 5. Reactor shielding materials. I. Jones, T. H. II. Scofield, N. E. III. Haggmark, L. G. IV. Gurney, W. J. V. Title. VI. SF Oll 05 11.</p> <p>UNCLASSIFIED</p>	<p>Naval Radiological Defense Laboratory USNRDL-TR-790</p> <p>EXPERIMENTAL DETERMINATION OF THE GAMMA-RAY ANGULAR DOSE ALBEDOS OF CONCRETE, ALUMINUM AND STEEL, by T. H. Jones, N. E. Scofield, L. G. Haggmark, and W. J. Gurney 6 October 1964 63 p. illus. tables 10 refs. UNCLASSIFIED</p> <p>The angular distribution of dose albedo was measured for "semi-infinite" concrete, aluminum and steel slabs irradiated by plane-parallel beams of Co<sup>60</sup> and Cs<sup>137</sup> gamma photons. The photons were incident on the slabs at angles, measured from a normal to the slab, of arccos 1.00, 0.75 and 0.50. For the necessary sensitivity, the reflected dose rate was</p> <p>(over)</p> <p>1. Gamma-ray scattering. 2. Steel - Bombardment. 3. Aluminum - Bombardment. 4. Concrete - Bombardment. 5. Reactor shielding materials. I. Jones, T. H. II. Scofield, N. E. III. Haggmark, L. G. IV. Gurney, W. J. V. Title. VI. SF Oll 05 11.</p> <p>UNCLASSIFIED</p>
<p>measured by a digital dosimetry system using a plastic scintillator as the detector.</p> <p>An empirical formula for angular dose albedo was derived from the experimental data. Comparisons are made with the Monte Carlo calculations of D. J. Raso and the experimental results of C. E. Clifford (DRCL).</p> <p>UNCLASSIFIED</p>	<p>measured by a digital dosimetry system using a plastic scintillator as the detector.</p> <p>An empirical formula for angular dose albedo was derived from the experimental data. Comparisons are made with the Monte Carlo calculations of D. J. Raso and the experimental results of C. E. Clifford (DRCL).</p> <p>UNCLASSIFIED</p>